Composites Part C: Open Access 2 (2020) 100038

Contents lists available at ScienceDirect

Composites Part C: Open Access

journal homepage: www.elsevier.com/locate/jcomc

Evaluation of exact electro-elastic static and free vibration solutions of multilayered plates for benchmarking: Piezoelectric composite laminates and soft core sandwich plates

F. Moleiro[a,*], C.M. Mota Soares[a], E. Carrera[b], J.N. Reddy[c]

[a] LAETA, IDMEC, Instituto Superior Técnico, Universidade de Lisboa, Av. Rovisco Pais 1, Lisboa 1049-001, Portugal
[b] Politecnico di Torino, Corso Duca degli Abruzzi 24, Torino 10129, Italy
[c] Texas A&M University, College Station, TX 77483-3123, USA

ARTICLE INFO

Keywords:
Multilayered plates
Electroelasticity
Three-dimensional exact solution
Piezoelectric layers
Composite layers

ABSTRACT

This work provides a study on three-dimensional exact electro-elastic static and free vibration solutions of multilayered plates, focused on a comprehensive evaluation of well-known benchmarks for piezoelectric and/or composite laminates as well as soft core sandwich plates, adding much to thus far available in the literature. The exact solution method for simply supported multilayered plates is fully described in line with earlier leading works, compiled in a single study in a consistent form throughout. The layers involved can be either piezoelectric layers poled through-thickness (i.e. *extension mode*) or purely elastic layers, including composite layers. For each layer, the form of the through-thickness exact solution depends strongly on its material properties, thus each case arising from an orthotropic, transversely isotropic or simply isotropic layer is considered specifically. Within the free vibration solution, in agreement with an in-plane mode (n_x, n_y), the so-called *special modes* for either $n_x = 0$ or $n_y = 0$, though often overlooked, are purposely addressed, along with *thickness modes* for each pair (n_x, n_y). The benchmarks cover purely elastic solutions, as in composite laminates and soft core sandwich plates, as well as electro-elastic solutions, namely piezoelectric composite laminates, involving not only but especially thick plates. For each multilayered plate, the static solution considers either an applied load or an applied electric potential, providing a detailed through-thickness evaluation of displacements and stresses, and when present, the electric potential and electric displacements. The respective free vibration solution reveals the first twenty natural frequencies and associated modes, including all together *special modes* and *thickness modes*.

1. Introduction

The advances of composite materials science alongside the ever-growing piezoelectric technology continues to drive forward structural design in a wide range of engineering applications. Over the years, in light of the increasing challenges posed to multilayered piezoelectric composite structures, three-dimensional (3D) exact solutions became paramount to assess the accuracy of various laminated plate and shell theories, along with related finite element models.

Early on, as composite laminates and sandwich plates started to raise interest, pioneer works on 3D exact elasticity solutions brought forth an immense knowledge on static and free vibration, all together, namely by Pagano [1], Pagano and Hatfield [2], Jones [3] as well as Srinivas and Rao [4], most notably. Later on, further advances on 3D exact solutions came to light to address additional effects, including electroelasticity and thermoelasticity. In line with the progress in smart structures technology, in which piezoelectric sensors and actuators continue to be most often favoured, 3D exact electroelasticity solutions provided far more insight into the behaviour of piezoelectric composite laminates. Specifically, the leading works on 3D exact static and free vibration solutions, first by Heyliger [5,6] and also Heyliger and Saravanos [7], considering embedded *extension mode* piezoelectric layers, followed by Vel and Batra [8] as well as Baillargeon and Vel [9], considering *shear mode* piezoelectric layers instead. Actually, in the scope of 3D exact free vibration solutions, the outstanding work by Batra and Aimmanee [10] is particularly noteworthy. It highlights that previous 3D exact solutions overlooked some in-plane modes of vibration (n_x, n_y), for either $n_x = 0$ or $n_y = 0$, addressing both composite laminates and piezoelectric plates, though only exploring *extension mode* piezoelectric layers. Soon after, Deü and Benjeddou [11] also examined such modes for either $n_x = 0$ or $n_y = 0$, named as *special modes*, in another remarkable work, in which *shear mode* piezoelectric layers are considered expressly. Beyond that,

* Corresponding author.
E-mail addresses: filipa.moleiro@tecnico.ulisboa.pt (F. Moleiro), cristovao.mota.soares@tecnico.ulisboa.pt (C.M. Mota Soares), erasmo.carrera@polito.it (E. Carrera), jnreddy@tamu.edu (J.N. Reddy).

https://doi.org/10.1016/j.jcomc.2020.100038
Received 15 July 2020; Accepted 2 September 2020

recognizing the critical effects of high temperature environments, 3D exact thermoelasticity solutions also emerged, including the primary work by Tungikar and Rao [12], shortly followed by further developments by Xu et al. [13,14] on 3D thermoelectroelasticity solutions. More recently, the usefulness of 3D exact electroelasticity solutions, as developed all together in the original works by Heyliger and Saravanos [5–7], gave rise to additional benchmarks for both static and free vibration, as pursued likewise by Moleiro et al. [15,16]. Furthermore, in line with cutting-edge structural design technology, the increasing attention to the effects of hygrothermal environments led to a quite novel work on 3D exact hygrothermal elasticity solutions, also by Moleiro et al. [17], addressing composite laminates, fibre metal laminates as well as sandwich plates.

Over time, comprehensive reviews on theories and computational models for multilayered composite plates and shells became available, relying much on established 3D exact solutions. Starting from the 1990s, with major reviews by Noor and Burton [18,19], Mallikarjuna and Kant [20], Reddy and Robbins [21] as well as Noor et al. [22], and by the turn of the century, leading to thorough reviews by Carrera [23–25] and the renowned book by Reddy [26]. Other than that, in light of the state-of-the-art of smart structures, further reviews on the modelling of piezoelectric composite laminates, in particular, also appeared around the same time. Specifically, the excellent reviews by Tang et al. [27], Saravanos and Heyliger [28], Gopinathan et al. [29], Benjeddou [30], Trindade and Benjeddou [31] and also Chopra [32], among others. In more recent times, as new developments arise through more refined theories and improved models, many more crucial assessments continue to come to light. Most noteworthy, the impressive book by Carrera et al. [33] in addition to some of the latest reviews by Liew et al. [34], Zhang et al. [35] and Li [36].

As demonstrated by the aforementioned reviews, benchmarks based on 3D exact solutions play a fundamental role in the assessment of any proposed model. In fact, some selected works in which established benchmarks for multilayered piezoelectric and/or composite plates are attentively reported may also be worth mentioning. Namely, on purely elastic modelling by Carrera and Demasi [37] as well as Moleiro et al. [38,39], on electro-elastic modelling by Heyliger et al. [40], Carrera et al. [41] and Moleiro et al. [42,43], and quite recently, on hygro-thermo-elastic modelling by Moleiro et al. [44].

This work provides a rather useful study on 3D exact electro-elastic static and free vibration solutions of multilayered plates, focused on a comprehensive evaluation of well-known benchmarks for piezoelectric and/or composite laminates as well as soft core sandwich plates, adding much to thus far available in the literature. Although not intended as a review, the exact solution method for simply supported multilayered plates is fully described in line with earlier leading works, compiled in a single study in a consistent form throughout. It considers *extension mode* piezoelectric layers and/or purely elastic layers, such as composite layers, including all particularities arising from an orthotropic, transversely isotropic or simply isotropic layer. The benchmarks for each multilayered plate cover both static and free vibration solutions. Most noteworthy, the static solution provides a detailed through-thickness evaluation of displacements and stresses, and when present, the electric potential and electric displacements, whereas the free vibration solution reveals the first twenty natural frequencies and associated modes, including all together *special modes* and *thickness modes*.

2. Electro-elastic problem governing equations

Consider, in general, the multilayered plate made of N layers, with a rectangular planar geometry $a \times b$ and a total thickness h, as represented in Fig. 1. In light of the 3D exact solution here described, the layers involved can be either piezoelectric layers poled through-thickness (i.e. *extension mode*) or purely elastic layers, including unidirectional fibre reinforced composite layers. In any case, the materials of the different layers can be orthotropic, transversely isotropic or simply isotropic, so long as the multilayered plate, as a whole, is kept orthotropic (at most).

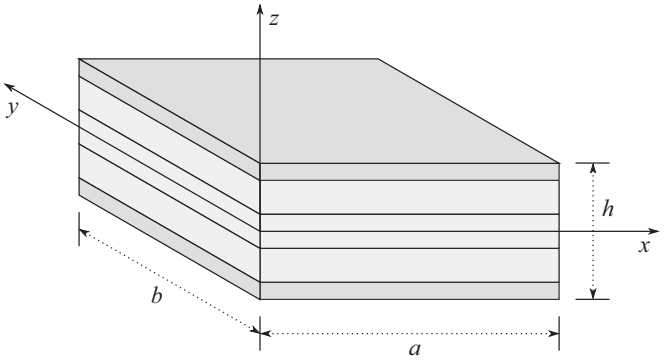

Fig. 1. Multilayered plate: geometry and coordinate system.

Hence, the orientation of orthotropic layers relative to the multilayered plate x-axis is limited to 0° and 90° alone.

In agreement with linear electroelasticity and assuming the absence of both electric body charges and body forces, the coupled governing equations for each layer of the multilayered plate are, all together, the following:

Equations of motion and charge equation of electrostatics

$$\frac{\partial \sigma_{ij}}{\partial x_j} = \rho \ddot{u}_i, \quad \frac{\partial D_i}{\partial x_i} = 0 \tag{1}$$

Electro-elastic constitutive equations

$$\begin{aligned} \sigma_{ij} &= C_{ijkl}\,\varepsilon_{kl} - e_{ijk}\,E_k \\ D_i &= e_{ikl}\,\varepsilon_{kl} + \epsilon_{ik}\,E_k \end{aligned} \tag{2}$$

Strain-displacement and electric field-potential equations

$$\varepsilon_{kl} = \frac{1}{2}\left(\frac{\partial u_k}{\partial x_l} + \frac{\partial u_l}{\partial x_k}\right), \quad E_k = -\frac{\partial \phi}{\partial x_k} \tag{3}$$

To be precise, the electric and elastic field variables in Eqs. (1)–(3) for each layer, along with its material coefficients are also described (including the respective SI units):

u_i	displacement vector components [m];
ϕ	electric (scalar) potential [V];
σ_{ij}	stress tensor components [Pa];
D_i	electric displacement vector components [C/m^2];
ε_{ij}	strain tensor components [dimensionless];
E_i	electric field vector components [V/m];
C_{ijkl}	elastic stiffness tensor coefficients [Pa];
e_{ijk}	piezoelectric tensor coefficients [C/m^2];
ϵ_{ij}	dielectric tensor coefficients [F/m].

Most often, the layer material coefficients are used in line with the contracted notation, such that the layer electro-elastic constitute equations are then expressed as shown:

$$\begin{aligned} \sigma_i &= C_{ij}\,\varepsilon_j - e_{ik}\,E_k \\ D_k &= e_{kj}\,\varepsilon_j + \epsilon_{kl}\,E_l \end{aligned} \tag{4}$$

where $i, j = 1, \ldots, 6$ and $k, l = 1, 2, 3$. As a result, notice that $\varepsilon_j = \varepsilon_{kl}$ for $k = l$ and $j = 1, 2, 3$, otherwise $\varepsilon_j = 2\varepsilon_{kl}$ for $k \neq l$ and $j = 4, 5, 6$.

Furthermore, in general, in view of an orthotropic layer with an orientation of either 0° or 90°, it is implied in the layer constitutive equations a prior in-plane rotation between the layer material coordinate system and the multilayered plate coordinate system (as necessary for the latter). See Reddy [26] for further details. Therefore, to denote clearly the layer rotated material coefficients, an overbar is used henceforth, as standard. Along with this, considering, in general, an *extension mode*

piezoelectric layer, the possible nonzero rotated material coefficients are the following: $\bar{C}_{11}$, $\bar{C}_{12}$, $\bar{C}_{13}$, $\bar{C}_{22}$, $\bar{C}_{23}$, $\bar{C}_{33}$, $\bar{C}_{44}$, $\bar{C}_{55}$ and $\bar{C}_{66}$ elastic stiffness coefficients; $\bar{e}_{31}$, $\bar{e}_{32}$, $\bar{e}_{33}$, $\bar{e}_{24}$ and $\bar{e}_{15}$ piezoelectric coefficients; $\bar{\epsilon}_{11}$, $\bar{\epsilon}_{22}$ and $\bar{\epsilon}_{33}$ dielectric coefficients (at most).

In short, substituting Eqs. (3) and (4) properly into Eq. (1) leads to four coupled governing equations for each layer of the multilayered plate, written only in terms of the displacements, u, v and w, and the electric potential ϕ, as follows:

$$\bar{C}_{11}\,u_{,xx} + \bar{C}_{12}\,v_{,xy} + \bar{C}_{13}\,w_{,xz} + \bar{e}_{31}\,\phi_{,xz} + \bar{C}_{66}\left(u_{,yy} + v_{,xy}\right) + \bar{C}_{55}\left(u_{,zz} + w_{,xz}\right) + \bar{e}_{15}\,\phi_{,yz} = \rho\ddot{u} \tag{5}$$

$$\bar{C}_{66}\left(u_{,xy} + v_{,xx}\right) + \bar{C}_{12}\,u_{,xy} + \bar{C}_{22}\,v_{,yy} + \bar{C}_{23}\,w_{,yz} + \bar{e}_{32}\,\phi_{,yz} + \bar{C}_{44}\left(v_{,zz} + w_{,yz}\right) + \bar{e}_{24}\,\phi_{,yz} = \rho\ddot{v} \tag{6}$$

$$\bar{C}_{55}\left(u_{,xz} + w_{,xx}\right) + \bar{e}_{15}\,\phi_{,xx} + \bar{C}_{44}\left(v_{,yz} + w_{,yy}\right) + \bar{e}_{24}\,\phi_{,yy} + \bar{C}_{13}\,u_{,xz} + \bar{C}_{23}\,v_{,yz} + \bar{C}_{33}\,w_{,zz} + \bar{e}_{33}\,\phi_{,zz} = \rho\ddot{w} \tag{7}$$

$$\bar{e}_{15}\left(u_{,xz} + w_{,xx}\right) - \bar{\epsilon}_{11}\,\phi_{,xx} + \bar{e}_{24}\left(v_{,yz} + w_{,yy}\right) - \bar{\epsilon}_{22}\,\phi_{,yy} + \bar{e}_{31}\,u_{,xz} + \bar{e}_{32}\,v_{,yz} + \bar{e}_{33}\,w_{,zz} - \bar{\epsilon}_{33}\,\phi_{,zz} = 0 \tag{8}$$

where, for conciseness, the comma is used to denote a partial derivative with respect to the adjacent spacial coordinates. Naturally, for the static solution all the time derivative terms are null, whereas for the free vibration solution a periodic response is assumed.

In fact, the 3D exact static and free vibration solution, as described here, is limited to simply supported multilayered plates with the following edge conditions:

$$\begin{aligned} &\text{At } x = 0, a: \; v = w = \phi = \sigma_{xx} = 0 \\ &\text{At } y = 0, b: \; u = w = \phi = \sigma_{yy} = 0 \end{aligned} \tag{9}$$

In addition, the boundary conditions on the multilayered plate top and bottom surfaces require the specification of one variable from each of the pairs: (u, σ_{xz}), (v, σ_{yz}), (w, σ_{zz}) and (ϕ, D_z); thus, in total, 8 boundary conditions for the top and bottom surfaces combined. Furthermore, the interfaces between adjacent layers are also assumed to be perfectly bonded together. Therefore, interlaminar continuity conditions must be enforced for each pair of adjacent layers with respect to all the following variables: u, v, w, ϕ, σ_{xz}, σ_{yz}, σ_{zz} and D_z; thus, for the entire multilayered plate made of N layers, in total, $8(N-1)$ interlaminar continuity conditions. In the end, considering all the aforementioned conditions brings forth $8N$ equations relating the electric and elastic field variables of all layers of the plate.

3. Exact static and free vibration solution method

In view of the rectangular simply supported multilayered plate, the general form of the 3D exact solution assumed for each layer displacements, u, v and w, and electric potential ϕ, such that it satisfies *a priori* the edge conditions stated in Eq. (9), is thus, as follows:

$$\begin{aligned} u &= \bar{u}(z)\exp(i\omega t)\cos(px)\sin(qy), & \bar{u}(z) &= \bar{U}\exp(sz) \\ v &= \bar{v}(z)\exp(i\omega t)\sin(px)\cos(qy), & \bar{v}(z) &= \bar{V}\exp(sz) \\ w &= \bar{w}(z)\exp(i\omega t)\sin(px)\sin(qy), & \bar{w}(z) &= \bar{W}\exp(sz) \\ \phi &= \bar{\phi}(z)\exp(i\omega t)\sin(px)\sin(qy), & \bar{\phi}(z) &= \bar{\Phi}\exp(sz) \end{aligned} \tag{10}$$

where $p = n_x\pi/a$ and $q = n_y\pi/b$. More precisely, the constants $\bar{U}$, $\bar{V}$, $\bar{W}$ and $\bar{\Phi}$ as well as the parameter s are to be determined by the solution of the coupled governing equations for each layer, given by Eqs. (5)–(8), together with the aforementioned boundary and interlaminar conditions. In line with the free vibration solution, ω denotes the frequency of natural vibration associated with the in-plane mode (n_x, n_y). In fact, for each pair (n_x, n_y), it exists infinite through-thickness modes, commonly known as *thickness modes*, which are also addressed herein. Moreover, the so-called *special modes* for either $n_x = 0$ or $n_y = 0$, though quite often overlooked by exact or analytical solutions, are purposely included as well.

Accordingly, substituting the assumed form of the layer 3D exact solution, as stated in Eq. (10), into its four coupled electro-elastic governing equations, given by Eqs. (5)–(8), leads to the following system of equations, for each layer:

$$\begin{bmatrix} A_{11}-\bar{C}_{55}s^2 & A_{12} & A_{13}s & A_{14}s \\ A_{12} & A_{22}-\bar{C}_{44}s^2 & A_{23}s & A_{24}s \\ -A_{13}s & -A_{23}s & A_{33}-\bar{C}_{33}s^2 & A_{34}-\bar{e}_{33}s^2 \\ -A_{14}s & -A_{24}s & A_{34}-\bar{e}_{33}s^2 & A_{44}+\bar{\epsilon}_{33}s^2 \end{bmatrix} \begin{Bmatrix} \bar{U} \\ \bar{V} \\ \bar{W} \\ \bar{\Phi} \end{Bmatrix} = \begin{Bmatrix} 0 \\ 0 \\ 0 \\ 0 \end{Bmatrix} \tag{11}$$

where

$$\begin{aligned} A_{11} &= \bar{C}_{11}p^2 + \bar{C}_{66}q^2 - \rho\,\omega^2 & A_{12} &= \left(\bar{C}_{12} + \bar{C}_{66}\right)p\,q \\ A_{22} &= \bar{C}_{66}p^2 + \bar{C}_{22}q^2 - \rho\,\omega^2, & A_{13} &= -\left(\bar{C}_{13} + \bar{C}_{55}\right)p \\ A_{33} &= \bar{C}_{55}p^2 + \bar{C}_{44}q^2 - \rho\,\omega^2, & A_{23} &= -\left(\bar{C}_{23} + \bar{C}_{44}\right)q \\ A_{34} &= \bar{e}_{15}p^2 + \bar{e}_{24}q^2, & A_{14} &= -\left(\bar{e}_{31} + \bar{e}_{15}\right)p \\ A_{44} &= -\bar{\epsilon}_{11}p^2 - \bar{\epsilon}_{22}q^2, & A_{24} &= -\left(\bar{e}_{32} + \bar{e}_{24}\right)q \end{aligned} \tag{12}$$

Furthermore, for the static solution, all the terms involving the frequency ω, as in $(-\rho\,\omega^2)$, are evidently disregarded, which may be considered simply as a particular case.

Therefore, for each layer, a non-trivial solution of the system in Eq. (11) requires a zero determinant. The resulting characteristic equation is an eighth-order polynomial involving only even powers of s, which can be rewritten as a fourth-order polynomial in terms of r, with $r = s^2$. The form of the through-thickness exact solution, for each layer, depends strongly on these 4 roots for r, as in 8 roots for s, which are associated with 8 (independent) unknown constants. Hence, for the entire multilayered plate made of N layers, in total, $8N$ unknown constants are to be determined by enforcing the aforementioned $8N$ boundary and interlaminar conditions. Most importantly, the roots for each layer are a function of its material properties and geometry, in addition to the frequency ω for the free vibration solution, which is then based on an iterative scheme, as described hereafter.

In any case, once the form of the through-thickness exact solution is properly defined for each layer displacements, u, v and w, and electric potential ϕ, in terms of its 8 roots for s and 8 unknown constants, in line with assumed form in Eq. (10), the corresponding exact solution form for each layer stresses and electric displacements are also set, according to the layer electro-elastic constitutive equations, along with the strain-displacement and electric field-potential equations, given by Eqs. (3) and (4), as shown:

$$\begin{aligned} \left(\sigma_{xz}, D_x\right) &= \left(\bar{\sigma}_{xz}(z), \bar{D}_x(z)\right)\exp(i\omega t)\cos(px)\sin(qy) \\ \left(\sigma_{yz}, D_y\right) &= \left(\bar{\sigma}_{yz}(z), \bar{D}_y(z)\right)\exp(i\omega t)\sin(px)\cos(qy) \\ \left(\sigma_{ii}, D_z\right) &= \left(\bar{\sigma}_{ii}(z), \bar{D}_z(z)\right)\exp(i\omega t)\sin(px)\sin(qy) \\ \sigma_{xy} &= \bar{\sigma}_{xy}(z)\exp(i\omega t)\cos(px)\cos(qy) \end{aligned} \tag{13}$$

where $i = 1, 2, 3$ is used for the layer normal stresses, σ_{xx}, σ_{yy} and σ_{zz}, and such that:

$$\begin{aligned} \bar{\sigma}_{xz}(z) &= \bar{C}_{55}\left(\bar{u}'(z) + p\,\bar{w}(z)\right) + \bar{e}_{15}\,p\,\bar{\phi}(z) \\ \bar{\sigma}_{yz}(z) &= \bar{C}_{44}\left(\bar{v}'(z) + q\,\bar{w}(z)\right) + \bar{e}_{24}\,q\,\bar{\phi}(z) \\ \bar{\sigma}_{xy}(z) &= \bar{C}_{66}(q\,\bar{u}(z) + p\,\bar{v}(z)) \\ \bar{\sigma}_{ii}(z) &= -p\,\bar{C}_{1i}\,\bar{u}(z) - q\,\bar{C}_{2i}\,\bar{v}(z) + \bar{C}_{3i}\,\bar{w}'(z) + \bar{e}_{3i}\,\bar{\phi}'(z) \end{aligned} \tag{14}$$

$$\begin{aligned} \bar{D}_x(z) &= \bar{e}_{15}\left(\bar{u}'(z) + p\,\bar{w}(z)\right) - \bar{\epsilon}_{11}\,p\,\bar{\phi}(z) \\ \bar{D}_y(z) &= \bar{e}_{24}\left(\bar{v}'(z) + q\,\bar{w}(z)\right) - \bar{\epsilon}_{22}\,q\,\bar{\phi}(z) \\ \bar{D}_z(z) &= -p\,\bar{e}_{31}\,\bar{u}(z) - q\,\bar{C}_{32}\,\bar{v}(z) + \bar{e}_{33}\,\bar{w}'(z) - \bar{\epsilon}_{33}\,\bar{\phi}'(z) \end{aligned} \tag{15}$$

Actually, for the static solution in particular, the terms involving the frequency ω, as in $\exp(i\omega t)$, appearing in the general form of Eqs. (10) and (13) are naturally omitted.

From this point on, in view of the simply supported multilayered plate made of N layers, the procedure for the static solution or the free

vibration solution is somewhat distinct. To begin with, the static solution is rather straightforward. For each layer, the form of the through-thickness exact solution is defined in terms of its 8 roots for s and 8 unknown constants, depending only on the layer material properties and geometry. Subsequently, the aforementioned $8N$ boundary and interlaminar conditions are enforced, all together, to determine the $8N$ unknown constants for each layer. The most common boundary conditions consider either an applied load $\hat{\sigma}_{zz}$ or an applied electric potential $\hat{\phi}$ on the multilayered plate top and/or bottom surfaces, with zero transverse shear stresses. To this end, the nonzero boundary conditions on the plate top and/or bottom surfaces are conveniently expressed in the form of double Fourier series, as follows:

$$\begin{aligned} \hat{\sigma}_{zz}(x,y) &= \sigma_0 \sin(px)\sin(qy) \\ \hat{\phi}(x,y) &= \phi_0 \sin(px)\sin(qy) \end{aligned} \tag{16}$$

Other than that, the free vibration solution is based on an iterative scheme, since the form of the through-thickness exact solution for each layer, namely its 8 roots for s, though still depending much on the layer material properties and geometry, are also a function of the frequency ω associated with the in-plane mode (n_x, n_y). Furthermore, the boundary conditions within the free vibration solution are all enforced as zero, including $\sigma_0 = 0$ and $\phi_0 = 0$. Hence, a non-trivial solution of the total system of $8N$ boundary and interlaminar conditions requires a zero determinant. In such case, the relationships among the electric and elastic field variables of all layers can be established, setting out the plate mode shapes in line with the pair (n_x, n_y) and the frequency ω.

In short, the iterative scheme relies on the evaluation of the determinant of the total system of $8N$ equations, using an estimated frequency in each iteration, in order to pursue a frequency of natural vibration leading to a zero determinant. The procedure is started with an estimated frequency somewhat lower than expected, which is then gradually increased in each iteration. In fact, the determinant is computed through the product of all eigenvalues of the total system matrix, to overcome numerical issues as the matrix becomes singular, as suggested by Heyliger and Saravanos [7]. More precisely, the iterative scheme keeps track of the determinant of the total system matrix and its lowest (absolute) eigenvalue to find a sign-change of the determinant together with a sign-change of the nearest zero eigenvalue. As a result, the estimated frequencies leading to the sign-changes can then be used as a bounding interval to refine the true value of the frequency of interest by a standard search method.

Most notably, for each pair (n_x, n_y), including *special modes* for either $n_x = 0$ or $n_y = 0$, it exists an infinite number of increasingly higher frequencies leading to a zero determinant, each associated with different *thickness modes*. Therefore, once one frequency is determined, the procedure can be restarted from then onwards, in order to pursue the next higher frequency leading to a zero determinant, corresponding to the next *thickness mode*.

Ultimately, at the core of both static and free vibration solution lies the form of the through-thickness exact solution for each layer, derived from a non-trivial solution of the system in Eq. (11). In fact, two distinct cases arise immediately: (*i*) *piezoelectric layers* with a fully coupled electro-elastic solution; and (*ii*) *purely elastic layers*, for which $\bar{e}_{ij} = 0$, with an uncoupled electric and elastic solution. Apart from that, one exceptional case is also envisioned, namely: (*iii*) *special modes* for either $n_x = 0$ or $n_y = 0$, emerging within the free vibration solution only. These three cases are addressed separately henceforth.

3.1. Piezoelectric layers: Orthotropic or transversely isotropic cases

For piezoelectric layers with a fully coupled electro-elastic solution, the characteristic equation of the system in Eq. (11) comes out, in its general form, as follows:

$$r^4 + c_1 r^3 + c_2 r^2 + c_3 r + c_4 = 0, \quad \text{with} \quad r = s^2 \tag{17}$$

where the coefficients c_i can be derived from the system in Eq. (11) by straightforward algebraic manipulation, although also presented, in some sense, by Heyliger and Saravanos [7].

For both static and free vibration solution, as it stands for piezoelectric layers, the nature of the 4 roots for r (with $r = s^2$) fall into one of two cases, depending mostly on the layer material properties:

- *4 real distinct roots*. Typically the case of piezoelectric layers of orthotropic material;
- *2 real distinct roots + 2 complex roots as a conjugate pair*. Typically the case of piezoelectric layers of transversely isotropic material.

In fact, the form of the through-thickness exact solution for each piezoelectric layer is defined based on the contribution of each root for s together with an associated unknown constant, usually of $\bar{u}(z)$, such that $\bar{v}(z)$, $\bar{w}(z)$ and $\bar{\phi}(z)$, are then set by making use of the remaining system of equations, as follows:

$$\begin{bmatrix} A_{22}-\bar{C}_{44}s^2 & A_{23}s & A_{24}s \\ -A_{23}s & A_{33}-\bar{C}_{33}s^2 & A_{34}-\bar{e}_{33}s^2 \\ -A_{24}s & A_{34}-\bar{e}_{33}s^2 & A_{44}+\bar{\epsilon}_{33}s^2 \end{bmatrix} \begin{Bmatrix} \bar{V} \\ \bar{W} \\ \bar{\Phi} \end{Bmatrix} = \bar{U} \begin{Bmatrix} -A_{12} \\ A_{13}s \\ A_{14}s \end{Bmatrix} \tag{18}$$

Accordingly, for a piezoelectric layer with n real distinct roots for r (with $r = s^2$), the roots for s appear as n distinct pairs (positive and negative), which are either real (if $r > 0$) or imaginary (if $r < 0$). Hence, following the approach of Heyliger and Savaranos [7], the form of the through-thickness exact solution for such piezoelectric layer, can be expressed (partially, at least), as shown:

$$\begin{aligned} \bar{u}(z) &= \sum_{j=1}^{n} U_j(z), \qquad \bar{w}(z) = \sum_{j=1}^{n} M_j W_j(z) \\ \bar{v}(z) &= \sum_{j=1}^{n} L_j U_j(z), \qquad \bar{\phi}(z) = \sum_{j=1}^{n} N_j W_j(z) \end{aligned} \tag{19}$$

where

$$\begin{aligned} U_j(z) &= F_j C_j(z) + G_j S_j(z) \\ W_j(z) &= G_j C_j(z) + \alpha_j F_j S_j(z) \end{aligned} \tag{20}$$

$$\begin{aligned} C_j(z) &= \cosh(m_j z), \quad S_j(z) = \sinh(m_j z), \quad \alpha_j = 1 \quad \text{if } r_j > 0 \\ C_j(z) &= \cos(m_j z), \quad S_j(z) = \sin(m_j z), \quad \alpha_j = -1 \quad \text{if } r_j < 0 \end{aligned} \tag{21}$$

and with $m_j = |r_j|^{1/2}$. In detail, F_j and G_j stand for the layer $2n$ (independent) unknown constants directly associated with $\bar{u}(z)$. As a result, the constants L_j, M_j and N_j associated with $\bar{v}(z)$, $\bar{w}(z)$ and $\bar{\phi}(z)$ can be readily set in agreement with the system in Eq. (18), as follows:

$$\begin{aligned} D_j &= d_1\alpha_j m_j^6 + d_2 m_j^4 + d_3\alpha_j m_j^2 + d_4 \\ L_j &= \left(f_{11}m_j^4 + f_{12}\alpha_j m_j^2 + f_{13}\right)/D_j \\ M_j &= \left(f_{21}m_j^4 + f_{22}\alpha_j m_j^2 + f_{23}\right)m_j/D_j \\ N_j &= \left(f_{31}m_j^4 + f_{32}\alpha_j m_j^2 + f_{33}\right)m_j/D_j \end{aligned} \tag{22}$$

where the coefficients d_i and f_{ij} can be derived from the system in Eq. (18) by straightforward algebraic manipulation, recognizing D_j as the determinant of the system matrix. Moreover, in view of the form of the through-thickness exact solution in Eq. (19), the corresponding derivatives with respect to z, necessary for the exact solution of the layer stresses and electric displacements, as stated in Eqs. (14) and (15), are then, the following:

$$\begin{aligned} \bar{u}'(z) &= \sum_{j=1}^{n} m_j W_j(z), \qquad \bar{w}'(z) = \sum_{j=1}^{n} \alpha_j m_j M_j U_j(z) \\ \bar{v}'(z) &= \sum_{j=1}^{n} m_j L_j W_j(z), \qquad \bar{\phi}'(z) = \sum_{j=1}^{n} \alpha_j m_j N_j U_j(z) \end{aligned} \tag{23}$$

Depending on the piezoelectric layer material properties, the total of real distinct roots for r is either $n = 4$ or $n = 2$, typically in line with an orthotropic or a transversely isotropic material, respectively. Therefore, if $n = 4$, Eq. (19) with $j = 1, \ldots, 4$ defines the layer through-thickness

exact solution completely, but if $n = 2$, Eq. (19) with $j = 1, 2$ describes only a partial solution, which requires additional terms to be summed with $j = 3, 4$, associated with 2 further complex roots for r as a conjugate pair.

In this latter case, for a piezoelectric layer with 2 complex roots for r as a conjugate pair (with $r = s^2$), the roots for s appear as 2 complex conjugate pairs in the form of $s = \pm(a \pm ib)$. Hence, the form of the through-thickness exact solution for such piezoelectric layer, can be developed based on $\bar{u}(z)$ expressed as shown:

$$\bar{u}(z) = \sum_{j=3}^{4} \left[F_j \hat{C}_j(z) + G_j \hat{S}_j(z) \right] \tag{24}$$

where F_j and G_j with $j = 3, 4$ denote the layer 4 additional (independent) unknown constants directly associated with $\bar{u}(z)$, as before, along with:

$$\begin{array}{l} \hat{C}_j(z) = \exp(\alpha_j a z)\cos(bz), \\ \hat{S}_j(z) = \exp(\alpha_j a z)\sin(bz), \end{array} \qquad \hat{\alpha}_j = \begin{cases} 1 & \text{if } j = 3 \\ -1 & \text{if } j = 4 \end{cases} \tag{25}$$

As a result, the relations concerning $\bar{v}(z)$, $\bar{w}(z)$ and $\bar{\phi}(z)$ can also be established in agreement with the system in Eq. (18), as follows:

$$\begin{array}{ll} \hat{D}(s) = d_1 s^6 + d_2 s^4 + d_3 s^2 + d_4 & \\ \hat{L}(s) = \left(f_{11} s^4 + f_{12} s^2 + f_{13}\right)/\hat{D}, & \bar{V} = \hat{L}\bar{U} \\ \hat{M}(s) = \left(f_{21} s^4 + f_{22} s^2 + f_{23}\right)/\hat{D}, & \bar{W} = s\hat{M}\bar{U} \\ \hat{N}(s) = \left(f_{31} s^4 + f_{32} s^2 + f_{33}\right)/\hat{D}, & \bar{\Phi} = s\hat{N}\bar{U} \end{array} \tag{26}$$

where the coefficients d_i and f_{ij} are precisely the same as in the previous Eq. (22), derived likewise from the system in Eq. (18). Since the roots for s are in the form of $s = \pm(a \pm ib)$, it is rather convenient to define, at once, the following related constants:

$$\begin{array}{ll} L_R = \Re(\hat{L}(a+ib)), & L_I = \Im(\hat{L}(a+ib)) \\ M_R = \Re(\hat{M}(a+ib)), & M_I = \Im(\hat{M}(a+ib)) \\ N_R = \Re(\hat{N}(a+ib)), & N_I = \Im(\hat{N}(a+ib)) \end{array} \tag{27}$$

Therefore, besides the expression of $\bar{u}(z)$ in Eq. (24), to begin with, the form of the through-thickness exact solution for such piezoelectric layer, following some algebraic manipulation, can be completed with the accompanying expression of $\bar{v}(z)$, $\bar{w}(z)$ and $\bar{\phi}(z)$, as shown:

$$\begin{aligned} \bar{v}(z) = \sum_{j=3}^{4} \Big[& F_j \Big(L_R \hat{C}_j(z) - L_I \hat{\alpha}_j \hat{S}_j(z) \Big) \\ & + G_j \Big(L_I \hat{\alpha}_j \hat{C}_j(z) + L_R \hat{S}_j(z) \Big) \Big] \end{aligned} \tag{28}$$

$$\begin{aligned} \bar{w}(z) = \sum_{j=3}^{4} \Big[& F_j \Big((aM_R - bM_I)\, \hat{\alpha}_j \hat{C}_j(z) - (aM_I + bM_R)\, \hat{S}_j(z) \Big) \\ & + G_j \Big((aM_I + bM_R)\, \hat{C}_j(z) + (aM_R - bM_I)\, \hat{\alpha}_j \hat{S}_j(z) \Big) \Big] \end{aligned} \tag{29}$$

$$\begin{aligned} \bar{\phi}(z) = \sum_{j=3}^{4} \Big[& F_j \Big((aN_R - bN_I)\, \hat{\alpha}_j \hat{C}_j(z) - (aN_I + bN_R)\, \hat{S}_j(z) \Big) \\ & + G_j \Big((aN_I + bN_R)\, \hat{C}_j(z) + (aN_R - bN_I)\, \hat{\alpha}_j \hat{S}_j(z) \Big) \Big] \end{aligned} \tag{30}$$

where it is used the functions $\hat{C}_j(z)$, $\hat{S}_j(z)$ and $\hat{\alpha}_j$ introduced in Eq. (25), along with the previous constants in Eq. (27). In fact, the form of the through-thickness exact solution, all together in Eqs. (24) and (28)–(30), is in line with Heyliger and Saravanos [7], although written here in a more compact form. Moreover, the corresponding derivatives with respect to z, necessary for the exact solution of the layer stresses and electric displacements, as stated in Eqs. (14) and (15), end up as given:

$$\begin{aligned} \bar{u}'(z) = \sum_{j=3}^{4} \Big[& F_j \Big(a\hat{\alpha}_j \hat{C}_j(z) - b\hat{S}_j(z) \Big) \\ & + G_j \Big(b\hat{C}_j(z) + a\hat{\alpha}_j \hat{S}_j(z) \Big) \Big] \end{aligned} \tag{31}$$

$$\begin{aligned} \bar{v}'(z) = \sum_{j=3}^{4} \Big[& F_j \Big((aL_R - bL_I)\, \hat{\alpha}_j \hat{C}_j(z) - (aL_I + bL_R)\, \hat{S}_j(z) \Big) \\ & + G_j \Big((aL_I + bL_R)\, \hat{C}_j(z) + (aL_R - bL_I)\, \hat{\alpha}_j \hat{S}_j(z) \Big) \Big] \end{aligned} \tag{32}$$

$$\begin{aligned} \bar{w}'(z) = \sum_{j=3}^{4} \Big[& F_j \Big(\left((a^2 - b^2)M_R - 2abM_I\right) \hat{C}_j(z) \\ & - \left((a^2 - b^2)M_I + 2abM_R\right) \hat{\alpha}_j \hat{S}_j(z) \Big) \\ & + G_j \Big(\left((a^2 - b^2)M_I + 2abM_R\right) \hat{\alpha}_j \hat{C}_j(z) \\ & + \left((a^2 - b^2)M_R - 2abM_I\right) \hat{S}_j(z) \Big) \Big] \end{aligned} \tag{33}$$

$$\begin{aligned} \bar{\phi}'(z) = \sum_{j=3}^{4} \Big[& F_j \Big(\left((a^2 - b^2)N_R - 2abN_I\right) \hat{C}_j(z) \\ & - \left((a^2 - b^2)N_I + 2abN_R\right) \hat{\alpha}_j \hat{S}_j(z) \Big) \\ & + G_j \Big(\left((a^2 - b^2)N_I + 2abN_R\right) \hat{\alpha}_j \hat{C}_j(z) \\ & + \left((a^2 - b^2)N_R - 2abN_I\right) \hat{S}_j(z) \Big) \Big] \end{aligned} \tag{34}$$

Most importantly, for a piezoelectric layer with the roots for r appearing as 2 real distinct roots and 2 complex roots as a conjugate pair, the complete form of the through-thickness exact solution includes the contribution of the solution form in Eq. (19) with $j = 1, 2$ related to the real roots, in addition to the solution form in Eqs. (24) and (28)–(30) with $j = 3, 4$ related to the complex roots instead.

3.2. Purely elastic layers: Orthotropic, transversely isotropic or isotropic cases

For purely elastic layers, for which $\bar{e}_{ij} = 0$, with an uncoupled electric and elastic solution, the characteristic equation of the system in Eq. (11) comes out, in its general form, as follows:

$$\left(r^3 + c_1 r^2 + c_2 r + c_3\right)\left(A_{44} + \bar{e}_{33} r\right) = 0, \quad \text{with} \quad r = s^2 \tag{35}$$

where the coefficients c_i can be derived from the system in Eq. (11) by straightforward algebraic manipulation, although also presented, in some sense, by Pagano [1].

Among the 4 roots for r, namely r_j with $j = 1, \ldots, 4$, the electric solution is naturally associated with *1 real uncoupled electric root*, which is simply $r_1 = -A_{44}/\bar{e}_{33}$ as in a positive real. Besides that, the nature of the remaining 3 roots for r, as it turns out for purely elastic layers, depends not only on the layer material properties but also on whether the static or free vibration solution is pursued.

For the static solution, the nature of the remaining 3 roots for r fall into one of two cases, depending on the layer material properties, in addition to *1 real uncoupled electric root*, whichever the case:

- *3 real distinct roots*. The case of purely elastic layers of orthotropic or transversely isotropic material;
- *3 real repeated roots*. The case of purely elastic layers of isotropic material.

For the free vibration solution, one of three cases arises instead, depending mostly on the layer material properties, in addition to *1 real uncoupled electric root*, whichever the case:

- *3 real distinct roots*. Typically the case of purely elastic layers of orthotropic material;
- *1 real root + 2 complex roots as a conjugate pair*. Typically the case of purely elastic layers of transversely isotropic material.
- *1 real root + 2 real repeated roots*. The case of purely elastic layers of isotropic material.

In most cases, for each purely elastic layer, the form of the elastic through-thickness exact solution is likewise defined based on the contribution of each root for s together with an associated unknown constant, usually of $\bar{u}(z)$, such that (if possible) $\bar{v}(z)$ and $\bar{w}(z)$, are then set through

the following system of equations:

$$\begin{bmatrix} A_{22}-\bar{C}_{44}s^2 & A_{23}s \\ -A_{23}s & A_{33}-\bar{C}_{33}s^2 \end{bmatrix} \begin{Bmatrix} \bar{V} \\ \bar{W} \end{Bmatrix} = \bar{U} \begin{Bmatrix} -A_{12} \\ A_{13}s \end{Bmatrix} \tag{36}$$

In view of a purely elastic layer with 1 real uncoupled electric root r_1, along with n real distinct elastic roots, as in $n = 3$ or $n = 1$ (with $r = s^2$), the corresponding roots for s appear as pairs (positive and negative), which are either real (if $r > 0$) or imaginary (if $r < 0$). Hence, the form of the through-thickness exact solution for such purely elastic layer, following the approach of Pagano [1] for the elastic part with $j = 2, \dots, n+1$, aside from the electric part with $j = 1$, can be expressed all together (partially, at least), as follows:

$$\begin{aligned} \bar{u}(z) &= \sum_{j=2}^{n+1} U_j(z), & \iota\bar{w}(z) &= \sum_{j=2}^{n+1} M_j W_j(z) \\ \bar{v}(z) &= \sum_{j=2}^{n+1} L_j U_j(z), & \bar{\phi}(z) &= \sum_{j=1}^{1} U_j(z) \end{aligned} \tag{37}$$

where it is used the functions $U_j(z)$ and $W_j(z)$ just as introduced earlier in Eqs. (20) and (21). As it stands, this solution form involves the layer (independent) unknown constants F_j and G_j with $j = 2, \dots, n+1$ directly associated with $\bar{u}(z)$, as well as F_1 and G_1 associated with $\bar{\phi}(z)$ alone. Accordingly, the constants L_j and M_j with $j = 2, \dots, n+1$ related to $\bar{v}(z)$ and $\iota\bar{w}(z)$ can be readily set in agreement with the system in Eq. (36), as shown:

$$\begin{aligned} D_j &= d_1 m_j^4 + d_2 \alpha_j m_j^2 + d_3 \\ L_j &= \left(f_{11}\alpha_j m_j^2 + f_{12} \right)/D_j \\ M_j &= \left(f_{21}\alpha_j m_j^2 + f_{22} \right) m_j/D_j \end{aligned} \tag{38}$$

where the coefficients d_i and f_{ij} can be derived likewise from the system in Eq. (36), recognizing once again D_j as the determinant of the system matrix. In addition, in line with the form of the through-thickness exact solution in Eq. (37), the derivatives with respect to z, necessary for the exact solution of the layer stresses and electric displacements, given in Eqs. (14) and (15), though simplified for $\bar{e}_{ij} = 0$, arise as given:

$$\begin{aligned} \bar{u}'(z) &= \sum_{j=2}^{n+1} m_j W_j(z), & \iota\bar{w}'(z) &= \sum_{j=2}^{n+1} \alpha_j m_j M_j U_j(z) \\ \bar{v}'(z) &= \sum_{j=2}^{n+1} m_j L_j W_j(z), & \bar{\phi}'(z) &= \sum_{j=1}^{1} m_j W_j(z) \end{aligned} \tag{39}$$

At this point, for such purely elastic layer, the total of real distinct elastic roots for r, as in $n = 3$ or $n = 1$, needs to be taken into account. If $n = 3$, Eq. (37) using $j = 1, \dots, 4$ defines the layer through-thickness exact solution completely, but if $n = 1$, Eq. (37) using $j = 1, 2$ describes only a partial solution, which requires additional terms to be summed for the elastic solution form using $j = 3, 4$.

Under this last case, one possibility is a purely elastic layer, typically transversely isotropic within the free vibration solution, with 1 real uncoupled electric root r_1, as well as for the elastic part, 1 real root r_2 (i.e. $n = 1$) and 2 further complex roots r_3 and r_4 as a conjugate pair (with $r = s^2$). Thus, the additional roots for s appear as 2 complex conjugate pairs in the form of $s = \pm(a \pm ib)$. Accordingly, the form of the elastic through-thickness exact solution involving the expression of $\bar{u}(z)$, $\bar{v}(z)$ and $\iota\bar{w}(z)$ with $j = 3, 4$ is given, in general, as stated in the previous Eqs. (24), (28) and (29), respectively, including the same functions $\hat{C}_j(z)$, $\hat{S}_j(z)$ and $\hat{a}_j$ introduced in Eq. (25), along with F_j and G_j as the layer 4 additional (independent) unknown constants directly associated with $\bar{u}(z)$. However, the distinction for this case of purely elastic layer lies in the fact that the constants L_R, L_I, M_R and M_I, appearing in the expression of $\bar{v}(z)$ and $\iota\bar{w}(z)$, need to be redefined appropriately. Since the elastic solution form is based on the expression of $\bar{u}(z)$, the corresponding relations concerning $\bar{v}(z)$ and $\iota\bar{w}(z)$ can be established in agreement with the system in Eq. (36), as follows:

$$\begin{aligned} &\hat{D}(s) = d_1 s^4 + d_2 s^2 + d_3 \\ &\hat{L}(s) = \left(f_{11}s^2 + f_{12} \right)/\hat{D}, \qquad \bar{V} = \hat{L}\bar{U} \\ &\hat{M}(s) = \left(f_{21}s^2 + f_{22} \right)/\hat{D}, \qquad \bar{W} = s\hat{M}\bar{U} \end{aligned} \tag{40}$$

where the coefficients d_i and f_{ij} are exactly the same as given in Eq. (38), derived likewise from the system in Eq. (36). In view of Eq. (40) with the roots for s in the form of $s = \pm(a \pm ib)$, the following related constants are thus redefined for this case of purely elastic layer:

$$\begin{aligned} L_R &= \Re(\hat{L}(a+ib)), & L_I &= \Im(\hat{L}(a+ib)) \\ M_R &= \Re(\hat{M}(a+ib)), & M_I &= \Im(\hat{M}(a+ib)) \end{aligned} \tag{41}$$

Moreover, the elastic solution derivatives with respect to z, necessary for the exact solution of the layer stresses and electric displacements, given in Eqs. (14) and (15) with $\bar{e}_{ij} = 0$, end up in the same general form as stated in the previous Eqs. (31)–(33), though using the constants L_R, L_I, M_R and M_I just set by Eqs. (40) and (41).

One other possibility is a purely elastic layer, namely isotropic within the free vibration solution, with 1 real uncoupled electric root r_1, as well as for the elastic part, 1 real root r_2 (i.e. $n = 1$) and 2 further real repeated roots $r_3 = r_4$ (with $r = s^2$). Therefore, the additional roots for s appear as 2 repeated pairs (positive and negative), which are either real (if $r > 0$) or imaginary (if $r < 0$). As it is, the form of the elastic through-thickness exact solution (associated with the roots $r_3 = r_4$) can be developed based on $\bar{u}(z)$, as shown:

$$\begin{aligned} \bar{u}(z) = \bar{v}(z) &= \textstyle\sum_{j=3}^{3} U_j(z) + \sum_{j=4}^{4} z\, U_j(z) \\ \iota\bar{w}(z) &= \textstyle\sum_{j=3}^{3} M_j W_j(z) + \sum_{j=4}^{4} \left[R_j U_j(z) + z\, M_j W_j(z) \right] \end{aligned} \tag{42}$$

where it is used the same functions $U_j(z)$ and $W_j(z)$ as defined in Eqs. (20) and (21), including F_j and G_j with $j = 3, 4$, which stand for the layer 4 additional (independent) unknown constants directly associated with $\bar{u}(z)$. Along with this, the constants M_j and R_j associated with $\iota\bar{w}(z)$ can be determined in view of the following elastic relation that also holds:

$$\left(A_{33} - \bar{C}_{33}s^2 \right)\bar{W} = \bar{U}s\left(A_{13} + A_{23} \right) \tag{43}$$

In fact, elastic independent equations arise, separately, according to the terms involving (z^0, z^1) of the solution form in Eq. (42), setting out the constants M_j with $j = 3, 4$ and R_j with $j = 4$, as follows:

$$\begin{aligned} D_j &= \left(-\bar{C}_{33} \right)\alpha_j m_j^2 + \left(A_{33} \right) \\ M_j &= \left(A_{13} + A_{23} \right) m_j/D_j, \quad \text{with } j = 3, 4 \\ R_j &= \left(\left(2M_j \bar{C}_{33} \right)\alpha_j m_j + \left(A_{13} + A_{23} \right) \right)/D_j, \quad \text{with } j = 4 \end{aligned} \tag{44}$$

In addition, in line with Eq. (42), the elastic solution derivatives with respect to z, necessary for the exact solution of the layer stresses and electric displacements, given in Eqs. (14) and (15) with $\bar{e}_{ij} = 0$, come out as given:

$$\begin{aligned} \bar{u}'(z) = \bar{v}'(z) &= \textstyle\sum_{j=3}^{3} m_j W_j(z) + \sum_{j=4}^{4} \left[U_j(z) + z\, m_j W_j(z) \right] \\ \iota\bar{w}'(z) &= \textstyle\sum_{j=3}^{3} \alpha_j m_j M_j U_j(z) \\ &\quad + \sum_{j=4}^{4} \left[\left(m_j R_j + M_j \right) W_j(z) + z\, \alpha_j m_j M_j U_j(z) \right] \end{aligned} \tag{45}$$

The only remaining possibility to consider is a purely elastic layer, namely isotropic within the static solution, with 1 real uncoupled electric root r_1, as well as for the elastic part, 3 real repeated roots $r_2 = r_3 = r_4$ (with $r = s^2$). Actually, in spite of the uncoupled electric and elastic solution, the roots for r turn out all equal, as in $r_j = c^2$ with $j = 1 \dots, 4$, such that $c^2 = p^2 + q^2$. Hence, the roots for s appear as real pairs $s = \pm c$, although 1 pair associated with the electric solution alone, and 3 repeated pairs associated with the elastic solution. As a result, the form of the elastic solution is quite distinctive for such purely elastic layer. Following the approach of Pagano [1] and also, more recently, Moleiro et al. [17], the through-thickness exact solution for the elastic part can

be expressed, in its general form, as follows:

$$\bar{X}_i(z) = \left(a_{1i} + a_{3i} z + a_{5i} z^2\right) \exp(cz) + \left(a_{2i} + a_{4i} z + a_{6i} z^2\right) \exp(-cz) \tag{46}$$

where $\bar{X}_i(z)$ with $i = 1, 2, 3$ stands for $\bar{u}(z)$, $\bar{v}(z)$ and $\bar{w}(z)$, respectively. More precisely, for such purely elastic layer, 8 (independent) unknown constants are involved, just like any other layer, including 2 (independent) unknown constants for the electric solution alone, thus 6 (independent) unknown constants for the elastic solution, among the 18 constants appearing in Eq. (46), as in a_{ki} with $k = 1, \ldots, 6$ and $i = 1, 2, 3$.

The relations among the 18 constants a_{ki} can be determined through the layer original system of equations for the elastic part, stated in Eq. (11), taking into account the isotropic layer material coefficients, and considering the various independent equations arising, separately, according to the terms involving $(z^0, z^1, z^2)\exp(\pm cz)$ of the elastic solution form in Eq. (46). In the end, taking as the 6 (independent) unknown constants the following: a_{11}, a_{21}, a_{31} and a_{41} from $\bar{u}(z)$, as well as a_{12} and a_{22} from $\bar{v}(z)$, the remaining constants become set as shown:

$$a_{5i} = a_{6i} = 0, \quad \text{with } i = 1, 2, 3 \tag{47}$$

$$a_{32} = \frac{q}{p} a_{31}, \quad a_{42} = \frac{q}{p} a_{41}, \quad a_{33} = \frac{c}{p} a_{31}, \quad a_{43} = -\frac{c}{p} a_{41} \tag{48}$$

$$a_{13} = \frac{p}{c} a_{11} + \frac{(C_{12} - 3C_{11})}{p(C_{11} + C_{12})} a_{31} + \frac{q}{c} a_{12} \tag{49}$$

$$a_{23} = -\frac{p}{c} a_{21} + \frac{(C_{12} - 3C_{11})}{p(C_{11} + C_{12})} a_{41} - \frac{q}{c} a_{22} \tag{50}$$

where the isotropic layer material coefficients involved C_{11} and C_{12} are such that:

$$\begin{aligned} \bar{C}_{11} &= \bar{C}_{22} = \bar{C}_{33} \equiv C_{11} \\ \bar{C}_{12} &= \bar{C}_{13} = \bar{C}_{23} \equiv C_{12} \\ \bar{C}_{44} &= \bar{C}_{55} = \bar{C}_{66} \equiv (C_{11} - C_{12})/2 \end{aligned} \tag{51}$$

Ultimately, the form of the through-thickness exact solution for such purely elastic layer, considering the uncoupled electric and elastic solution all together, with the roots for s as real pairs $s = \pm c$, can be written as follows:

$$\bar{X}_i(z) = \left(a_{1i} + a_{3i}\, z\right) \exp(cz) + \left(a_{2i} + a_{4i}\, z\right) \exp(-cz) \tag{52}$$

$$\bar{\phi}(z) = \sum_{j=1}^{1} U_j(z) = \sum_{j=1}^{1} \left[F_j C_j(z) + G_j S_j(z)\right] \tag{53}$$

where $\bar{X}_i(z)$ with $i = 1, 2, 3$ stands again for $\bar{u}(z)$, $\bar{v}(z)$ and $\bar{w}(z)$, respectively, along with the functions $C_j(z)$ and $S_j(z)$ with $j = 1$ for $\bar{\phi}(z)$ alone, as introduced in Eqs. (20) and (21). In short, the layer solution form involves 8 (independent) unknown constants, namely F_1 and G_1 for the electric solution alone, in addition to the aforementioned 6 (independent) unknown constants for the elastic solution. Other than that, the remaining constants for the elastic solution are set by Eqs. (47)–(50).

Furthermore, the corresponding solution derivatives with respect to z, necessary for the layer stresses and electric displacements, given in Eqs. (14) and (15) with $\bar{e}_{ij} = 0$, end up as shown:

$$\bar{X}_i'(z) = \left(a_{3i} + c\, a_{1i} + c\, a_{3i}\, z\right) \exp(cz) + \left(a_{4i} - c\, a_{2i} - c\, a_{4i}\, z\right) \exp(-cz) \tag{54}$$

$$\bar{\phi}'(z) = \sum_{j=1}^{1} m_j W_j(z) = \sum_{j=1}^{1} m_j \left[G_j C_j(z) + \alpha_j F_j S_j(z)\right] \tag{55}$$

where $\bar{X}_i'(z)$ with $i = 1, 2, 3$ is used accordingly for $\bar{u}'(z)$, $\bar{v}'(z)$ and $\bar{w}'(z)$, aside from the functions $C_j(z)$ and $S_j(z)$ with $j = 1$, as before, for $\bar{\phi}'(z)$ only, though here including explicitly $m_j = |r_j|^{1/2}$ as in $m_1 = c$ for such purely elastic layer.

In sum, for each layer, whether piezoelectric or purely elastic, the appropriate form of the through-thickness exact solution can be defined, as thoroughly described, whichever the case arising from the layer material properties, according to an orthotropic, transversely isotropic or even isotropic layer. Most noteworthy, thus far, each of the above-mentioned solution form holds under any pair (n_x, n_y), so long as neither $n_x = 0$ nor $n_y = 0$.

3.3. Special modes: $n_x = 0$ or $n_y = 0$ cases

Within the free vibration solution, the so-called *special modes* for either $n_x = 0$ or $n_y = 0$ fall into a particular case, which needs to be addressed separately, each on its own. In case $n_x = 0$, meaning $p = 0$, the characteristic equation of the system in Eq. (11) turns out, in its general form, as follows:

$$\left(r^3 + c_1 r^2 + c_2 r + c_3\right)\left(A_{11} - \bar{C}_{55} r\right) = 0, \quad \text{with} \quad r = s^2 \tag{56}$$

Evidently, when $n_x = 0$, the form of the through-thickness exact solution, for each and every layer, is such that the displacement $\bar{u}(z)$ emerges uncoupled. Hence, for each layer, among the 4 roots for r, namely r_j with $j = 1, \ldots, 4$, the solution form of $\bar{u}(z)$ is clearly associated with just *1 real uncoupled root*, which is simply $r_1 = A_{11}/\bar{C}_{55}$. The remaining 3 roots for r can be all real roots or include complex roots, as in a conjugate pair, depending mostly on the layer material properties. Accordingly, the form of the through-thickness exact solution for each layer can be developed along the same lines as described previously. Nonetheless, the aftermath shows that, when $n_x = 0$, the solution form of $\bar{v}(z)$, $\bar{w}(z)$ and $\bar{\phi}(z)$ are all null, and only the layer displacement $\bar{u}(z)$ is nonzero. This holds for either purely elastic layers or the present *extension mode* piezoelectric layers, as indeed highlighted by Batra and Aimmanee [10]. Most notably, this solution form of *special modes* for $n_x = 0$ is only admissible under simply supported edge conditions at $x = 0, a$, as given by Eq. (9).

Therefore, in such case, the form of the through-thickness exact solution rests on $\bar{u}(z)$ for every layer, each with 1 real uncoupled root r_1 (with $r = s^2$), thus 1 pair of roots for s (positive and negative). As it is, the solution form of $\bar{u}(z)$ for each layer, as well as its derivative with respect to z, can be expressed as shown:

$$\begin{aligned} \bar{u}(z) &= \textstyle\sum_{j=1}^{1} U_j(z) = \sum_{j=1}^{1} \left[F_j C_j(z) + G_j S_j(z)\right] \\ \bar{u}'(z) &= \textstyle\sum_{j=1}^{1} m_j W_j(z) = \sum_{j=1}^{1} m_j \left[G_j C_j(z) + \alpha_j F_j S_j(z)\right] \end{aligned} \tag{57}$$

where it is used the functions $U_j(z)$ and $W_j(z)$ as defined in Eqs. (20) and (21), including explicitly $m_j = |r_j|^{1/2}$ with $j = 1$ for each layer, along with its 2 unknown constants F_1 and G_1 associated with $\bar{u}(z)$ alone. As a result, when $n_x = 0$, the solution form for each layer stresses and electric displacements, as stated originally in Eqs. (14) and (15), is simply reduced to the following:

$$\begin{aligned} \bar{\sigma}_{xz}(z) &= \bar{C}_{55}\, \bar{u}'(z) \\ \bar{\sigma}_{xy}(z) &= q\, \bar{C}_{66}\, \bar{u}(z) \\ \bar{D}_x(z) &= \bar{e}_{15}\, \bar{u}'(z) \end{aligned} \tag{58}$$

Other than that, in case $n_y = 0$, meaning $q = 0$, the characteristic equation of the system in Eq. (11) turns out, in its general form, as follows:

$$\left(r^3 + c_1 r^2 + c_2 r + c_3\right)\left(A_{22} - \bar{C}_{44} r\right) = 0, \quad \text{with} \quad r = s^2 \tag{59}$$

Analogously, when $n_y = 0$, the form of the through-thickness exact solution, for each and every layer, is such that the displacement $\bar{v}(z)$ emerges uncoupled. Naturally, for each layer, the solution form of $\bar{v}(z)$ is associated with just *1 real uncoupled root*, namely $r_1 = A_{22}/\bar{C}_{44}$. Likewise, the aftermath shows that, when $n_y = 0$, the solution form of $\bar{u}(z)$, $\bar{w}(z)$ and $\bar{\phi}(z)$ are all null, and only the layer displacement $\bar{v}(z)$ is nonzero. Therefore, this solution form of *special modes* for $n_y = 0$ is only admissible under simply supported edge conditions at $y = 0, b$, as given by Eq. (9). In such case, the form of the through-thickness exact solution rests on $\bar{v}(z)$ for every layer, each with 1 real uncoupled root r_1 (with

Table 1
Elastic properties of the materials used for purely elastic solutions.

Property	FRC [1]	Trans. Iso. Core [1]	Iso. Core [17]
E_1 [GPa]	$25E_0$	$0.04E_0$	$0.04E_0$
E_2 [GPa]	E_0†	$0.04E_0$	$0.04E_0$
E_3 [GPa]	E_0†	$0.5E_0$	$0.04E_0$
G_{12} [GPa]	$0.5E_0$	$0.016E_0$	$E_0/70$
G_{13} [GPa]	$0.5E_0$	$0.06E_0$	$E_0/70$
G_{23} [GPa]	$0.2E_0$	$0.06E_0$	$E_0/70$
ν_{12} [-]	0.25	0.25	0.40
ν_{13} [-]	0.25	0.02	0.40
ν_{23} [-]	0.25	0.02	0.40
ρ [kg/m^3]	ρ_0†	$0.1\rho_0$	$0.1\rho_0$

[3] For nondimensionalizations. Used as $E_0 = 7$ GPa and $\rho_0 = 1600$ kg/m^3.

$r = s^2$), thus 1 pair of roots for s (positive and negative). Equivalently, the solution form of $\bar{v}(z)$ and $\bar{v}'(z)$ for each layer, can be expressed just as stated in Eq. (57), respectively.

Besides that, when $n_y = 0$, the solution form for each layer stresses and electric displacements, as stated in Eqs. (14) and (15), is reduced accordingly to the following:

$$\begin{aligned} \bar{\sigma}_{yz}(z) &= \bar{C}_{44}\,\bar{v}'(z) \\ \bar{\sigma}_{xy}(z) &= p\,\bar{C}_{66}\,\bar{v}(z) \\ \bar{D}_y(z) &= \bar{e}_{24}\,\bar{v}'(z) \end{aligned} \tag{60}$$

In the end, from a practical standpoint, when considering *special modes* for either $n_x = 0$ or $n_y = 0$ within the free vibration solution, the nonzero exact solution form for each layer involves, in fact, only 2 nonzero unknown constants F_1 and G_1. Hence, for the entire multilayered plate made of N layers, only $2N$ nonzero unknown constants are actually involved. Accordingly, taking into account for each layer, in reality, only 1 nonzero displacement and 1 nonzero transverse shear stress, leads all together to the corresponding $2N$ boundary and interlaminar conditions. In short, in case of *special modes* for either $n_x = 0$ or $n_y = 0$, the free vibration solution can be based on a reduced total system of $2N$ equations, whose zero determinant requirement is pursued through an iterative scheme, as described earlier, thus setting out the plate *special mode* shapes in line with the pair (n_x, n_y) and the respective frequency ω.

4. Static and free vibration solutions for benchmarking

As intended in this work, 3D exact electro-elastic static and free vibration solutions of simply supported multilayered plates are demonstrated by a comprehensive evaluation of well-known benchmarks, divided into two categories: purely elastic solutions and electro-elastic solutions. Specifically, within each category, three distinct square multilayered plates (with $a = b$) are studied, as here described.

1. *Purely elastic solutions*, using the materials in Table 1:
   - *Composite laminate* (0°/90°/0°).
     Considering unidirectional fibre reinforced composite (FRC) layers of equal thickness $h/3$ and $a/h = 4, 10, 100$; based on the original benchmark by Pagano [1], in which exact static solutions are shown, in part.
   - *Sandwich plate with transversely isotropic soft core*.
     Considering FRC skins of 0° with thickness $h/10$ (each) alongside a soft core and $a/h = 4, 10, 100$; based on the original benchmark by Pagano [1], in which exact static solutions are shown, in part.
   - *Sandwich plate with isotropic soft core*.
     An analogous sandwich using a distinct core material; based on the original benchmark by Moleiro et al. [17], though modified here to assume the same thickness layout as the previous sandwich.
2. *Electro-elastic solutions*, using the materials in Table 2:
   - *Piezoelectric composite laminate* (PZT-4/0°/90°/PZT-4).
     Considering piezoelectric layers with thickness $h/10$ (each) alongside FRC layers of equal thickness, with a fixed total thickness $h = 1$ m and $a/h = 4, 10$; based on the original benchmark by Heyliger [5], in which exact static solutions are shown, in part.
   - *Piezoelectric composite laminate* (PZT-4/0°/90°/0°/PZT-4).
     Considering piezoelectric layers with thickness $h/10$ (each) alongside FRC layers of equal thickness, with a fixed total thickness $h = 0.01$ m and $a/h = 4, 10$; based on the original benchmark by Heyliger and Saravanos [7], in which exact free vibration solutions are shown, in part.
   - *Piezoelectric composite laminate* (PVDF/90°/0°/90°/PVDF).
     An analogous laminate using a distinct piezoelectric material, namely PVDF of 0°, with the same thickness layout as the previous laminate; based on the original benchmark by Heyliger et al. [40], in which exact static solutions are shown, in part.

Table 2
Elastic and piezoelectric properties of the materials used for electro-elastic solutions.

Property	FRC [7]	PZT-4 [7]	PVDF [7]
E_1 [GPa]	132.38	81.3	237.0
E_2 [GPa]	10.756	81.3	23.2
E_3 [GPa]	10.756	64.5	10.5
G_{12} [GPa]	5.6537	30.6	6.43
G_{13} [GPa]	5.6537	25.6	4.40
G_{23} [GPa]	3.6060	25.6	2.15
ν_{12} [-]	0.24	0.329	0.154
ν_{13} [-]	0.24	0.432	0.178
ν_{23} [-]	0.49	0.432	0.177
e_{31} [C/m^2]	0	-5.20	-0.13
e_{32} [C/m^2]	0	-5.20	-0.14
e_{33} [C/m^2]	0	15.08	-0.28
e_{24} [C/m^2]	0	12.72	-0.01
e_{15} [C/m^2]	0	12.72	-0.01
ϵ_{11} [F/m]	$3.5\epsilon_0$†	$1475\epsilon_0$	$12.50\epsilon_0$
ϵ_{22} [F/m]	$3.0\epsilon_0$†	$1475\epsilon_0$	$11.98\epsilon_0$
ϵ_{33} [F/m]	$3.0\epsilon_0$†	$1300\epsilon_0$	$11.98\epsilon_0$
ρ [kg/m^3]	1.0	1.0	1.0

° The vacuum dielectric constant. Used as $\epsilon_0 = 8.854187817 \times 10^{-12}$ F/m.

Moreover, within purely elastic solutions, following primarily the leading work by Pagano [1], 3D exact static and free vibration solutions are provided in a nondimensionalized form, which is most useful for future assessments. Accordingly, exact static solutions of all displacements and stresses make use of the following nondimensionalized form:

$$\begin{aligned} [\tilde{u}, \tilde{v}] &= \frac{100E_0h^2}{\sigma_0 a^3}[u, v], \quad \tilde{w} = \frac{100E_0h^3}{\sigma_0 a^4}w \\ \left[\tilde{\sigma}_{xz}, \tilde{\sigma}_{yz}\right] &= \frac{h}{\sigma_0 a}\left[\sigma_{xz}, \sigma_{yz}\right], \quad \tilde{\sigma}_{zz} = \frac{\sigma_{zz}}{\sigma_0} \\ \left[\tilde{\sigma}_{xx}, \tilde{\sigma}_{yy}, \tilde{\sigma}_{xy}\right] &= \frac{h^2}{\sigma_0 a^2}\left[\sigma_{xx}, \sigma_{yy}, \sigma_{xy}\right] \end{aligned} \tag{61}$$

From a practical standpoint, the exact static solutions in this form hold for each side-to-thickness ratio a/h considered, in line with the elastic property reference E_0 in Table 1 and the applied load intensity σ_0 stated in Eq. (16). Along with this, exact free vibration solutions of all natural frequencies are also provided in nondimensionalized form, as shown:

$$\tilde{\omega} = \omega\sqrt{\rho_0/E_0}\left(a^2/h\right) \tag{62}$$

Likewise, the natural frequencies in this form hold as well for each side-to-thickness ratio a/h considered, in agreement with both E_0 and ρ_0, as in the density reference in Table 1.

Furthermore, 3D exact static solutions, within purely elastic or electro-elastic solutions, consider (as suitable) either a bi-sinusoidal applied load of intensity σ_0 or a bi-sinusoidal applied electric potential of intensity ϕ_0 on the plate top surface, according to Eq. (16) with $p = q = \pi/a$, along with all zero loads on the plate bottom surface. More specifically, within electro-elastic static solutions, a unit value is as-

Table 3
Exact static solutions of the composite laminate (0°/90°/0°) under an applied load (nondimensionalized); in part, shown by Pagano [1].

a/h	z/h	$\tilde{u}(0,\frac{a}{2})$	$\tilde{v}(\frac{a}{2},0)$	$\tilde{w}(\frac{a}{2},\frac{a}{2})$	$\tilde{\sigma}_{xz}(0,\frac{a}{2})$	$\tilde{\sigma}_{yz}(\frac{a}{2},0)$	$\tilde{\sigma}_{zz}(\frac{a}{2},\frac{a}{2})$	$\tilde{\sigma}_{xx}(\frac{a}{2},\frac{a}{2})$	$\tilde{\sigma}_{yy}(\frac{a}{2},\frac{a}{2})$	$\tilde{\sigma}_{xy}(0,0)$
4	1/2	−0.9694	−2.2812	2.1216	0.0000	0.0000	1.0000	0.8008	0.0953	−0.0511
	1/6	0.3167	−0.6637	2.0416	0.2518	0.0892	0.7184	−0.2301	0.0298	−0.0055
	1/6	0.3167	−0.6637	2.0416	0.2518	0.0892	0.7184	0.0066	0.5341	−0.0055
	0	0.0521	0.0269	2.0059	0.2559	0.2172	0.4927	0.0059	−0.0119	0.0012
	−1/6	−0.2418	0.7156	1.9803	0.2570	0.0758	0.2691	0.0062	−0.5563	0.0074
	−1/6	−0.2418	0.7156	1.9803	0.2570	0.0758	0.2691	0.1900	−0.0164	0.0074
	−1/2	0.9358	2.2794	1.9381	0.0000	0.0000	0.0000	−0.7548	−0.0792	0.0505
10	1/2	−0.7351	−1.0995	0.7533	0.0000	0.0000	1.0000	0.5906	0.0429	−0.0288
	1/6	−0.0943	−0.3574	0.7537	0.3532	0.0478	0.7371	0.0794	0.0139	−0.0071
	1/6	−0.0943	−0.3574	0.7537	0.3532	0.0478	0.7371	0.0076	0.2845	−0.0071
	0	0.0036	0.0044	0.7530	0.3573	0.1228	0.4994	0.0011	−0.0019	0.0001
	−1/6	0.1007	0.3661	0.7521	0.3543	0.0457	0.2620	−0.0054	−0.2882	0.0073
	−1/6	0.1007	0.3661	0.7521	0.3543	0.0457	0.2620	−0.0814	−0.0117	0.0073
	−1/2	0.7380	1.1066	0.7485	0.0000	0.0000	0.0000	−0.5898	−0.0407	0.0290
100	1/2	−0.6780	−0.6823	0.4347	0.0000	0.0000	1.0000	0.5393	0.0269	−0.0214
	1/6	−0.2243	−0.2274	0.4347	0.3905	0.0336	0.7407	0.1784	0.0089	−0.0071
	1/6	−0.2243	−0.2274	0.4347	0.3905	0.0336	0.7407	0.0089	0.1808	−0.0071
	0	0.0000	0.0000	0.4347	0.3947	0.0828	0.5000	0.0000	0.0000	0.0000
	−1/6	0.2244	0.2274	0.4347	0.3905	0.0336	0.2593	−0.0089	−0.1808	0.0071
	−1/6	0.2244	0.2274	0.4347	0.3905	0.0336	0.2593	−0.1784	−0.0089	0.0071
	−1/2	0.6781	0.6823	0.4347	0.0000	0.0000	0.0000	−0.5393	−0.0268	0.0214

Table 4
Exact static solutions of the sandwich plate with transversely isotropic soft core under an applied load (nondimensionalized); in part, shown by Pagano [1].

a/h	z/h	$\tilde{u}(0,\frac{a}{2})$	$\tilde{v}(\frac{a}{2},0)$	$\tilde{w}(\frac{a}{2},\frac{a}{2})$	$\tilde{\sigma}_{xz}(0,\frac{a}{2})$	$\tilde{\sigma}_{yz}(\frac{a}{2},0)$	$\tilde{\sigma}_{zz}(\frac{a}{2},\frac{a}{2})$	$\tilde{\sigma}_{xx}(\frac{a}{2},\frac{a}{2})$	$\tilde{\sigma}_{yy}(\frac{a}{2},\frac{a}{2})$	$\tilde{\sigma}_{xy}(0,0)$
4	1/2	−1.8785	−7.2672	7.8137	0.0000	0.0000	1.0000	1.5558	0.2595	−0.1437
	2/5	0.3690	−4.9825	7.8129	0.2354	0.1007	0.9307	−0.2331	0.1687	−0.0725
	2/5	0.3690	−4.9825	7.8129	0.2354	0.1007	0.9307	0.0027	0.0081	−0.0023
	0	0.1406	0.3109	7.5962	0.2387	0.1072	0.5002	0.0005	0.0004	0.0002
	−2/5	−0.3016	5.3996	7.5030	0.2364	0.1013	0.0689	−0.0013	−0.0070	0.0026
	−2/5	−0.3016	5.3996	7.5030	0.2364	0.1013	0.0689	0.1963	−0.1666	0.0801
	−1/2	1.8446	7.5805	7.4653	0.0000	0.0000	0.0000	−1.5121	−0.2533	0.1480
10	1/2	−1.4299	−3.0689	2.2033	0.0000	0.0000	1.0000	1.1531	0.1104	−0.0707
	2/5	−0.7699	−2.3892	2.2056	0.2974	0.0493	0.9407	0.6279	0.0837	−0.0496
	2/5	−0.7699	−2.3892	2.2056	0.2974	0.0493	0.9407	0.0021	0.0037	−0.0016
	0	0.0050	0.0352	2.2004	0.2998	0.0527	0.5002	0.0001	0.0001	0.0000
	−2/5	0.7742	2.4540	2.1977	0.2977	0.0495	0.0594	−0.0018	−0.0035	0.0016
	−2/5	0.7742	2.4540	2.1977	0.2977	0.0495	0.0594	−0.6287	−0.0832	0.0507
	−1/2	1.4315	3.1309	2.1944	0.0000	0.0000	0.0000	−1.1518	−0.1099	0.0717
100	1/2	−1.3799	−1.3994	0.8924	0.0000	0.0000	1.0000	1.0975	0.0550	−0.0437
	2/5	−1.0998	−1.1191	0.8924	0.3221	0.0279	0.9430	0.8748	0.0439	−0.0349
	2/5	−1.0998	−1.1191	0.8924	0.3221	0.0279	0.9430	0.0019	0.0019	−0.0011
	0	0.0000	0.0003	0.8924	0.3240	0.0297	0.5000	0.0000	0.0000	0.0000
	−2/5	1.0999	1.1198	0.8924	0.3221	0.0279	0.0570	−0.0018	−0.0019	0.0011
	−2/5	1.0999	1.1198	0.8924	0.3221	0.0279	0.0570	−0.8748	−0.0439	0.0349
	−1/2	1.3799	1.4001	0.8924	0.0000	0.0000	0.0000	−1.0975	−0.0550	0.0437

sumed for either intensities, as in $\sigma_0 = 1$ Pa or $\phi_0 = 1$ V, in order to be consistent with the leading works by Heyliger [5] as well as Heyliger et al. [40].

4.1. Purely elastic solutions: Composite laminates and soft core sandwich plates

Firstly, 3D exact static solutions are shown in Tables 3,4,5 regarding, respectively, the composite laminate (0°/90°/0°) and each of the two sandwich plates with soft core, all equally under a bi-sinusoidal applied load. In each table, the exact static solutions provide a detailed through-thickness evaluation of all displacements and stresses, in nondimensionalized form as established by Eq. (61), considering three distinct side-to-thickness ratios $a/h = 4, 10, 100$, thus including thick, moderately thick and even thin plates.

In fact, the original benchmarks by Pagano [1] concerning both the composite laminate (0°/90°/0°) and the sandwich plate with transversely isotropic soft core are here much more thoroughly described in Tables 3 and 4, with the evaluation of all displacements and stresses at the top and bottom surfaces of each layer of the plate, and also in the mid-surface, in sequence, for each side-to-thickness ratio considered. Actually, this comprehensive evaluation is done likewise in Table 5 concerning the sandwich plate with isotropic soft core.

Other than that, a more insightful description of the static behaviour of each multilayered plate can be provided by the exact through-thickness distributions of displacements and stresses, all together. Since both original benchmarks by Pagano [1] are more widely known, this further description seems most relevant at this point for the sandwich plate with isotropic soft core, as shown in Fig. 2, thus characterizing its static behaviour. More precisely, Fig. 2 demonstrates the exact through-thickness distributions of displacements and stresses, considering alongside each side-to-thickness ratio $a/h = 4, 10, 100$.

As apparent in Fig. 2 the through-thickness distributions exhibit much more complicated effects when thick sandwich plates are considered, and even heighten by a soft core. Naturally, an accurate modelling of sandwich plates must be able to capture all of such through-thickness

Table 5
Exact static solutions of the sandwich plate with isotropic soft core under an applied load (nondimensionalized).

a/h	z/h	$\tilde{u}(0,\frac{a}{2})$	$\tilde{v}(\frac{a}{2},0)$	$\tilde{w}(\frac{a}{2},\frac{a}{2})$	$\tilde{\sigma}_{xz}(0,\frac{a}{2})$	$\tilde{\sigma}_{yz}(\frac{a}{2},0)$	$\tilde{\sigma}_{zz}(\frac{a}{2},\frac{a}{2})$	$\tilde{\sigma}_{xx}(\frac{a}{2},\frac{a}{2})$	$\tilde{\sigma}_{yy}(\frac{a}{2},\frac{a}{2})$	$\tilde{\sigma}_{xy}(0,0)$
4	1/2	−4.0865	−10.689	24.338	0.0000	0.0000	1.0000	3.3213	0.3846	−0.2321
	2/5	3.2657	−3.2566	24.339	0.1568	0.1107	0.9039	−2.5280	0.0912	0.0001
	2/5	3.2657	−3.2566	24.339	0.1568	0.1107	0.9039	0.0347	0.0406	0.0000
	0	2.5515	3.7181	22.801	0.1849	0.1417	0.5241	0.0158	0.0147	0.0028
	−2/5	−2.7869	6.3026	21.952	0.1943	0.1455	0.1018	0.0046	−0.0035	0.0016
	−2/5	−2.7869	6.3026	21.952	0.1943	0.1455	0.1018	2.1467	−0.1749	0.0552
	−1/2	3.8044	12.927	21.900	0.0000	0.0000	0.0000	−3.0972	−0.4371	0.2628
10	1/2	−1.7017	−6.0228	5.6548	0.0000	0.0000	1.0000	1.3904	0.2056	−0.1213
	2/5	0.0432	−4.2680	5.6588	0.2472	0.0831	0.9352	0.0025	0.1364	−0.0664
	2/5	0.0432	−4.2680	5.6588	0.2472	0.0831	0.9352	0.0087	0.0126	−0.0019
	0	0.0815	0.3212	5.6407	0.2557	0.0938	0.5055	0.0031	0.0028	0.0002
	−2/5	−0.0161	4.7822	5.6057	0.2546	0.0900	0.0669	−0.0024	−0.0067	0.0021
	−2/5	−0.0161	4.7822	5.6057	0.2546	0.0900	0.0669	−0.0248	−0.1503	0.0749
	−1/2	1.7113	6.5185	5.6004	0.0000	0.0000	0.0000	−1.3987	−0.2188	0.1293
100	1/2	−1.3804	−1.4600	0.9365	0.0000	0.0000	1.0000	1.0984	0.0569	−0.0446
	2/5	−1.0865	−1.1659	0.9365	0.3209	0.0286	0.9429	0.8647	0.0453	−0.0354
	2/5	−1.0865	−1.1659	0.9365	0.3209	0.0286	0.9429	0.0024	0.0025	−0.0010
	0	0.0001	0.0026	0.9366	0.3231	0.0308	0.5001	0.0000	0.0000	0.0000
	−2/5	1.0867	1.1711	0.9365	0.3210	0.0287	0.0571	−0.0023	−0.0024	0.0010
	−2/5	1.0867	1.1711	0.9365	0.3210	0.0287	0.0571	−0.8649	−0.0454	0.0355
	−1/2	1.3806	1.4652	0.9365	0.0000	0.0000	0.0000	−1.0986	−0.0570	0.0447

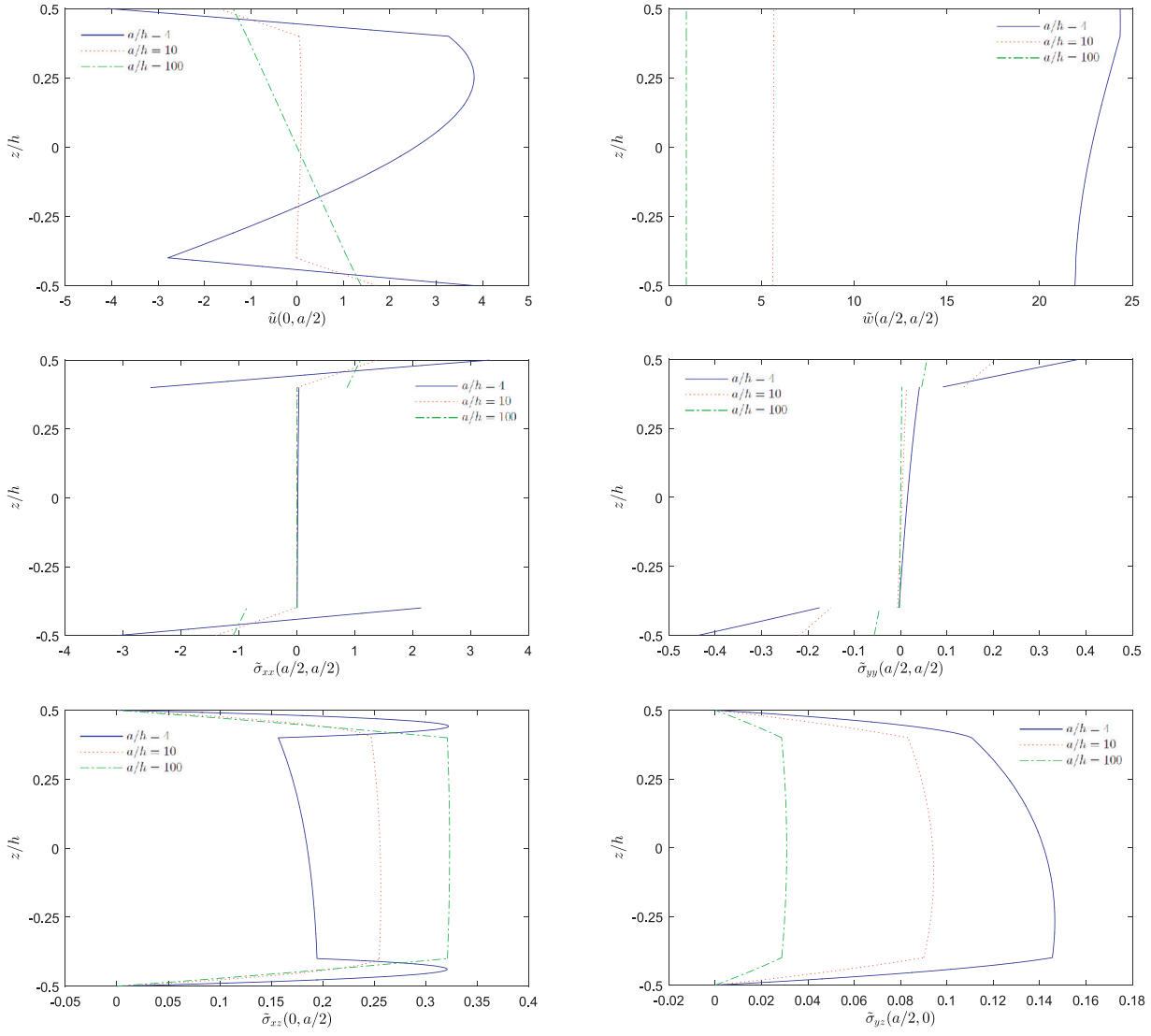

Fig. 2. Exact static solutions of the sandwich plate with isotropic soft core under an applied load, using $a/h = 4, 10, 100$: through-thickness distributions of displacements and stresses (nondimensionalized).

Table 6
Exact free vibration solutions of the composite laminate (0°/90°/0°): first twenty natural frequencies (nondimensionalized) and associated modes (n_x, n_y)–N_z (in-plane mode and thickness mode number).

	$\bar{\omega}_1$	$\bar{\omega}_2$	$\bar{\omega}_3$	$\bar{\omega}_4$	$\bar{\omega}_5$	$\bar{\omega}_6$	$\bar{\omega}_7$	$\bar{\omega}_8$	$\bar{\omega}_9$	$\bar{\omega}_{10}$
a/h	$\bar{\omega}_{11}$	$\bar{\omega}_{12}$	$\bar{\omega}_{13}$	$\bar{\omega}_{14}$	$\bar{\omega}_{15}$	$\bar{\omega}_{16}$	$\bar{\omega}_{17}$	$\bar{\omega}_{18}$	$\bar{\omega}_{19}$	$\bar{\omega}_{20}$
4	6.9161	8.8858	8.8858	11.5417	14.0593	16.8943	17.7539	17.7715	17.7715	21.6489
	(1,1)–1	**(0,1)**–1	**(1,0)**–1	(1,2)–1	(2,1)–1	(2,2)–1	(1,3)–1	**(0,2)**–1	**(2,0)**–1	(2,3)–1
	21.8020	23.7802	24.3201	26.6573	26.6573	27.0272	27.3102	27.3922	29.3163	29.4744
	(3,1)–1	(3,2)–1	(1,4)–1	**(0,3)**–1	**(3,0)**–1	**(0,1)**–**2**	(2,4)–1	(3,3)–1	**(1,0)**–**2**	(1,1)–**2**
10	11.4573	18.2120	22.2144	22.2144	28.1818	30.5643	31.8919	40.5370	44.4288	44.4288
	(1,1)–1	(1,2)–1	**(0,1)**–1	**(1,0)**–1	(2,1)–1	(1,3)–1	(2,2)–1	(2,3)–1	**(0,2)**–1	**(2,0)**–1
	45.6518	46.3135	48.8648	53.0403	55.0841	61.9544	64.9684	65.2176	66.6432	66.6432
	(1,4)–1	(3,1)–1	(3,2)–1	(2,4)–1	(3,3)–1	(1,5)–1	(3,4)–1	(4,1)–1	**(0,3)**–1	**(3,0)**–1

Table 7
Exact free vibration solutions of the sandwich plate with transversely isotropic soft core: first twenty natural frequencies (nondimensionalized) and associated modes (n_x, n_y)–N_z (in-plane mode and thickness mode number).

	$\bar{\omega}_1$	$\bar{\omega}_2$	$\bar{\omega}_3$	$\bar{\omega}_4$	$\bar{\omega}_5$	$\bar{\omega}_6$	$\bar{\omega}_7$	$\bar{\omega}_8$	$\bar{\omega}_9$	$\bar{\omega}_{10}$
a/h	$\bar{\omega}_{11}$	$\bar{\omega}_{12}$	$\bar{\omega}_{13}$	$\bar{\omega}_{14}$	$\bar{\omega}_{15}$	$\bar{\omega}_{16}$	$\bar{\omega}_{17}$	$\bar{\omega}_{18}$	$\bar{\omega}_{19}$	$\bar{\omega}_{20}$
4	6.7059	7.9661	7.9665	10.8667	12.8849	13.8219	15.5166	16.3804	15.8704	15.8739
	(1,1)–1	**(1,0)**–1	**(0,1)**–1	(1,2)–1	(2,1)–1	(1,1)–**2**	(2,2)–1	(1,3)–1	**(2,0)**–1	**(0,2)**–1
	19.4201	19.7453	19.9399	20.1002	20.1919	21.7811	22.1463	23.6399	23.6523	23.7642
	(2,1)–**2**	(2,3)–1	(3,1)–1	**(1,0)**–**2**	**(0,1)**–**2**	(3,2)–1	(1,4)–1	**(3,0)**–1	**(0,3)**–1	(1,2)–**2**
10	12.6425	18.6896	19.9361	19.9362	28.1824	29.8259	31.7268	34.6661	39.5603	39.8484
	(1,1)–1	(1,2)–1	**(1,0)**–1	**(0,1)**–1	(2,1)–1	(1,3)–1	(2,2)–1	(1,1)–**2**	(2,3)–1	**(2,0)**–1
	39.8497	43.4986	43.9708	46.6039	48.8918	50.7665	52.4464	58.2430	59.7124	59.7170
	(0,2)–1	(1,4)–1	(3,1)–1	(3,2)–1	(2,1)–**2**	(2,4)–1	(3,3)–1	(1,5)–1	**(3,0)**–1	**(0,3)**–1

Table 8
Exact free vibration solutions of the sandwich plate with isotropic soft core: first twenty natural frequencies (nondimensionalized) and associated modes (n_x, n_y)–N_z (in-plane mode and thickness mode number).

	$\bar{\omega}_1$	$\bar{\omega}_2$	$\bar{\omega}_3$	$\bar{\omega}_4$	$\bar{\omega}_5$	$\bar{\omega}_6$	$\bar{\omega}_7$	$\bar{\omega}_8$	$\bar{\omega}_9$	$\bar{\omega}_{10}$
a/h	$\bar{\omega}_{11}$	$\bar{\omega}_{12}$	$\bar{\omega}_{13}$	$\bar{\omega}_{14}$	$\bar{\omega}_{15}$	$\bar{\omega}_{16}$	$\bar{\omega}_{17}$	$\bar{\omega}_{18}$	$\bar{\omega}_{19}$	$\bar{\omega}_{20}$
4	3.9816	6.2393	7.6986	7.8822	7.8827	8.8764	8.9849	11.2201	11.8853	12.3319
	(1,1)–1	(1,2)–1	(2,1)–1	**(1,0)**–1	**(0,1)**–1	(2,2)–1	(1,3)–1	(2,3)–1	(1,4)–1	**(1,0)**–**2**
	12.3394	13.0277	13.7064	13.9733	14.9071	15.1467	15.4493	15.4537	16.4588	17.4374
	(0,1)–**2**	(3,1)–1	(2,4)–1	(3,2)–1	(1,5)–1	(3,3)–1	**(2,0)**–1	**(0,2)**–1	(2,5)–1	(3,4)–1
10	9.5920	12.8150	15.5812	19.6029	19.6576	19.8010	19.8011	23.9314	24.2850	26.5655
	(1,1)–1	(1,2)–1	(2,1)–1	(2,2)–1	(1,3)–1	**(1,0)**–1	**(0,1)**–1	(2,3)–1	(3,1)–1	(3,2)–1
	26.9739	30.2100	30.4055	34.2412	34.3893	35.6415	36.0171	36.9740	39.0782	39.4944
	(1,4)–1	(2,4)–1	(3,3)–1	(4,1)–1	(1,5)–1	(3,4)–1	(4,2)–1	(2,5)–1	(4,3)–1	**(2,0)**–1

effects, namely the zig-zag form of displacements and the interlaminar continuity of transverse stresses. In short, this can be translated into C_z^0 interlaminar continuity requirements of displacements and transverse stresses, as highlighted early on by Carrera [23–25].

In addition, 3D exact free vibration solutions are shown in Tables 6,7,8 regarding, once again respectively, the composite laminate (0°/90°/0°) and each of the two sandwich plates with soft core. In each table, the free vibration solutions reveal the first twenty natural frequencies, in nondimensionalized form as stated by Eq. (62), along with the associated modes of natural vibration, considering two distinct side-to-thickness ratios $a/h = 4, 10$, thus including both thick and moderately thick plates. More specifically, for each natural frequency, the corresponding in-plane mode (n_x, n_y) is reported, which also includes *special modes* for either $n_x = 0$ or $n_y = 0$, together with the *thickness mode* number of each pair (n_x, n_y).

As shown in Tables 6,7,8, the *special modes* are, in fact, a significant part of the first twenty natural modes of vibration of each (simply supported) multilayered plate, and even more so when thick plates are considered. As it turns out, for thick plates most notably, among the first twenty modes of vibration of each multilayered plate, about six up to eight modes correspond to *special modes*, although, as the plate becomes less thick, this proportion of *special modes* among the first twenty modes of vibration tends to decrease somewhat. Actually, the lower natural frequencies corresponding to *special modes*, namely either the pair (0,1) or (1,0), can occur immediately as the second lowest natural frequency when thick plates are considered, as demonstrated in Tables 6 and 7. Therefore, even though often overlooked, the significance of *special modes* for thick (simply supported) multilayered plates is quite undeniable, as emphasized first by Batra and Aimmanee [10]. Moreover, Tables 6,7,8 also reveal, for thick plates most especially, that for each pair (n_x, n_y) at least up to the second *thickness mode* can appear among the first twenty modes of vibration of each multilayered plate, thus it cannot be disregarded. In fact, for each thick plate considered, about two up to five modes of vibration among the first twenty modes correspond to a second *thickness mode*. This is particularly pronounced in the free vibration behaviour of the sandwich plate with transversely isotropic soft core, as shown in Table 7 and further characterized in Fig. 3.

In more detail, Fig. 3 focuses on a few modes of natural vibration to bring light into the first few through-thickness mode shapes of each in-plane mode (n_x, n_y). It includes for the in-plane mode (1,1), the first three *thickness modes* of the transverse displacement w, and likewise for the in-plane mode (2,1), the first two *thickness modes*. As demonstrated in Fig. 3, for each in-plane mode, such as (1,1) or (2,1), the natural modes of vibration from the second *thickness mode* onwards, rather expose the transverse normal compressibility of the sandwich plate, as mostly due to its soft core. Aside from that, Fig. 3 also includes, for the *special mode* (1,0), the first two *thickness modes* of the in-plane displace-

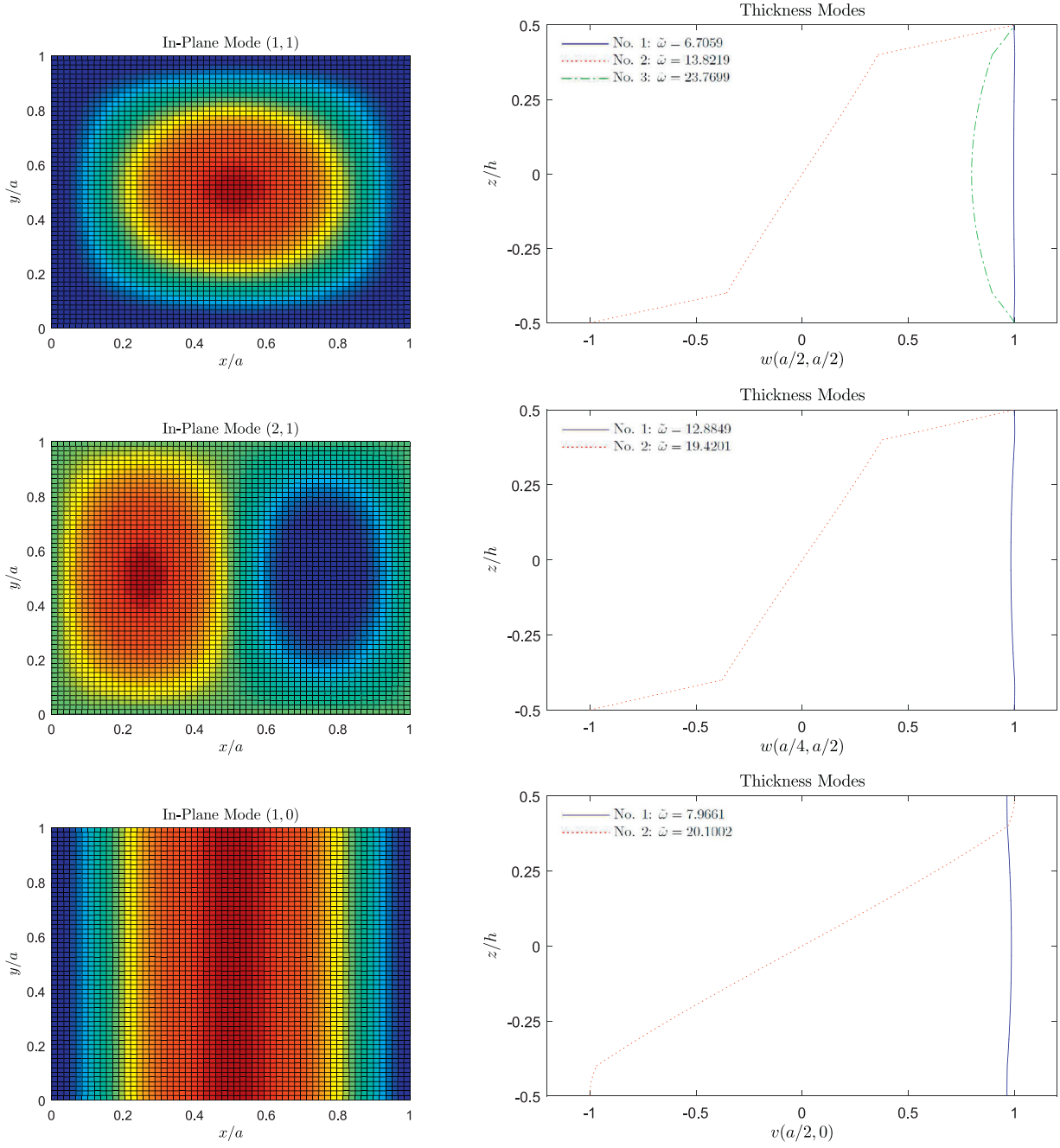

Fig. 3. Exact free vibration solutions of the sandwich plate with transversely isotropic soft core, using $a/h = 4$: a few natural frequencies (nondimensionalized) and associated modes, characterizing the first few through-thickness modes of each in-plane mode.

ment *v*. Thus, apparently, for each *special mode*, such as (1,0) or (0,1), the natural modes of vibration from the second *thickness mode* onwards, further expose the effect of transverse shear of the sandwich plate, as arising mainly from its soft core.

Most noteworthy, comparing the free vibration behaviour of both sandwich plates, reported in Tables 7 and 8, which differ only on the core material, as detailed in Table 1, clearly indicates that the degree of the core compressibility plays a key role on the occurrence of higher *thickness modes* among the lower natural frequencies. In short, the significance of *thickness modes*, from the second onwards, among the first twenty, or more, modes of vibration of any multilayered plate is apparently greatly influenced by the degree of sensitivity to the effects of transverse shear and normal compressibility of the plate. This gives reason to the relevance of *thickness modes* when thick plates are considered, and most especially sandwich plates exhibiting high core compressibility.

4.2. Electro-elastic solutions: Piezoelectric composite laminates

The following 3D exact electro-elastic static solutions of each of the three piezoelectric composite laminates, under either a bi-sinusoidal applied load or a bi-sinusoidal applied electric potential (of a unit value), are now shown in a series of six tables, namely Tables 9,10,11,12,13,14, every two tables for each laminate in line with either sensor or actuator configuration, respectively.

Table 9
Exact static solutions of the piezoelectric composite laminate (PZT-4/0°/90°/PZT-4) under an applied load (in SI units); in part, shown by Heyliger [5].

a/h	z/h	$u \cdot 10^{12}$ $(0, \frac{a}{2})$	$v \cdot 10^{12}$ $(\frac{a}{2}, 0)$	$w \cdot 10^{11}$ $(\frac{a}{2}, \frac{a}{2})$	$\phi \cdot 10$ $(\frac{a}{2}, \frac{a}{2})$	$\sigma_{xz} \cdot 10$ $(0, \frac{a}{2})$	$\sigma_{yz} \cdot 10$ $(\frac{a}{2}, 0)$	$\sigma_{zz} \cdot 10$ $(\frac{a}{2}, \frac{a}{2})$	σ_{xx} $(\frac{a}{2}, \frac{a}{2})$	σ_{yy} $(\frac{a}{2}, \frac{a}{2})$	σ_{xy} $(0, 0)$	$D_x \cdot 10^{12}$ $(0, \frac{a}{2})$	$D_y \cdot 10^{12}$ $(\frac{a}{2}, 0)$	$D_z \cdot 10^{13}$ $(\frac{a}{2}, \frac{a}{2})$
4	1/2	−55.506	−47.552	31.525	0.0000	0.0000	0.0000	10.000	6.9464	6.5642	−2.4768	0.0000	0.0000	160.58
	2/5	−31.746	−23.733	31.761	0.0598	5.7901	5.4892	9.5153	4.0258	3.6408	−1.3334	196.60	181.65	−0.3384
	2/5	−31.746	−23.733	31.761	0.0598	5.7901	5.4892	9.5153	0.7907	2.8857	−0.2464	−0.1249	−0.1457	−0.3384
	0	−12.064	20.394	30.029	0.0611	7.7429	6.8712	4.9831	0.3085	−1.9267	0.0370	−0.1274	−0.1487	0.5053
	0	−12.064	20.394	30.029	0.0611	7.7429	6.8712	4.9831	1.3977	0.0991	0.0370	−0.1487	−0.1274	0.5053
	−2/5	25.619	39.313	28.766	0.0756	5.4609	5.9752	0.4867	−2.7387	−0.3617	0.2883	−0.1840	−0.1578	1.4590
	−2/5	25.619	39.313	28.766	0.0756	5.4609	5.9752	0.4867	−3.5769	−4.2348	1.5605	156.24	181.80	1.4590
	−1/2	47.089	60.683	28.428	0.0000	0.0000	0.0000	0.0000	−6.2126	−6.8658	2.5901	0.0000	0.0000	−142.46
10	1/2	−929.59	−552.49	578.94	0.0000	0.0000	0.0000	10.000	40.023	32.776	−14.248	0.0000	0.0000	139.12
	2/5	−750.11	−372.56	580.91	0.4434	15.129	12.851	9.5404	31.287	24.031	−10.793	481.75	368.57	−0.4125
	2/5	−750.11	−372.56	580.91	0.4434	15.129	12.851	9.5404	3.3243	16.521	−1.9940	−0.3700	−0.4317	−0.4125
	0	−212.98	227.27	582.15	0.4448	18.923	18.542	5.0065	0.7867	−9.1428	0.0254	−0.3712	−0.4330	0.5936
	0	−212.98	227.27	582.15	0.4448	18.923	18.542	5.0065	8.8940	−0.3492	0.0254	−0.4330	−0.3712	0.5936
	−2/5	383.45	764.08	577.96	0.4614	12.939	15.235	0.4625	−16.628	−2.8835	2.0382	−0.4492	−0.3850	1.6201
	−2/5	383.45	764.08	577.96	0.4614	12.939	15.235	0.4625	−24.103	−31.418	11.031	361.99	476.09	1.6201
	−1/2	562.43	942.61	575.89	0.0000	0.0000	0.0000	0.0000	−32.802	−40.109	14.468	0.0000	0.0000	−135.96

Table 10
Exact static solutions of the piezoelectric composite laminate (PZT-4/0°/90°/PZT-4) under an applied potential (in SI units); in part, shown by Heyliger [5].

a/h	z/h	$u \cdot 10^{12}$ $(0, \frac{a}{2})$	$v \cdot 10^{12}$ $(\frac{a}{2}, 0)$	$w \cdot 10^{12}$ $(\frac{a}{2}, \frac{a}{2})$	ϕ $(\frac{a}{2}, \frac{a}{2})$	$\sigma_{xz} \cdot 10^{3}$ $(0, \frac{a}{2})$	$\sigma_{yz} \cdot 10^{3}$ $(\frac{a}{2}, 0)$	$\sigma_{zz} \cdot 10^{3}$ $(\frac{a}{2}, \frac{a}{2})$	$\sigma_{xx} \cdot 10^{2}$ $(\frac{a}{2}, \frac{a}{2})$	$\sigma_{yy} \cdot 10^{2}$ $(\frac{a}{2}, \frac{a}{2})$	$\sigma_{xy} \cdot 10^{2}$ $(0, 0)$	$D_x \cdot 10^{10}$ $(0, \frac{a}{2})$	$D_y \cdot 10^{10}$ $(\frac{a}{2}, 0)$	$D_z \cdot 10^{11}$ $(\frac{a}{2}, \frac{a}{2})$
4	1/2	−28.002	−32.765	−16.058	1.0000	0.0000	0.0000	0.0000	88.918	111.80	−146.04	−152.21	−152.21	−241.84
	2/5	9.5340	4.7353	−13.956	0.9929	38.247	56.266	−7.5347	−102.91	−79.852	34.294	−150.94	−150.85	−4.1875
	2/5	9.5340	4.7353	−13.956	0.9929	38.247	56.266	−7.5347	−9.4310	−51.677	6.3361	−0.2071	−0.2417	−4.1875
	0	2.7374	0.0297	−14.707	0.4477	8.2398	−23.857	−14.605	−3.0553	−1.3928	1.2287	−0.0934	−0.1090	−3.1825
	0	2.7374	0.0297	−14.707	0.4477	8.2398	−23.857	−14.605	−29.126	−1.3087	1.2287	−0.1090	−0.0934	−3.1825
	−2/5	−0.7427	−1.7835	−14.415	−0.0001	−19.463	−23.371	−1.8720	8.0547	1.5720	−1.1217	0.0000	0.0000	−2.8702
	−2/5	−0.7427	−1.7835	−14.415	−0.0001	−19.463	−23.371	−1.8720	9.5233	14.524	−6.0713	−0.0809	−0.1003	−2.8702
	−1/2	−1.8287	−2.8618	−14.246	0.0000	0.0000	0.0000	0.0000	22.821	27.784	−11.273	0.0000	0.0000	−2.7935
10	1/2	−12.022	−13.407	−13.912	1.0000	0.0000	0.0000	0.0000	14.141	16.803	−24.445	−60.885	−60.885	−41.680
	2/5	3.1351	1.7484	−13.533	0.9987	2.6520	3.4886	−0.1956	−16.999	−14.334	4.6946	−60.791	−60.787	−3.4653
	2/5	3.1351	1.7484	−13.533	0.9987	2.6520	3.4886	−0.1956	−1.2165	−7.5678	0.8674	−0.0833	−0.0972	−3.4653
	0	1.2395	0.0398	−13.697	0.4910	0.9355	−1.9643	−0.3946	−0.4437	−0.2816	0.2272	−0.0410	−0.0478	−3.2966
	0	1.2395	0.0398	−13.697	0.4910	0.9355	−1.9643	−0.3946	−5.1966	−0.1341	0.2272	−0.0478	−0.0410	−3.2966
	−2/5	−0.4221	−1.4665	−13.664	0.0002	−1.0165	−1.6466	−0.0466	1.8816	0.5299	−0.3354	0.0000	0.0000	−3.2409
	−2/5	−0.4221	−1.4665	−13.664	0.0002	−1.0165	−1.6466	−0.0466	−0.0175	1.9895	−1.8156	−0.0148	−0.0179	−3.2409
	−1/2	−0.8469	−1.8900	−13.596	0.0000	0.0000	0.0000	0.0000	2.0456	4.0503	−2.6310	0.0000	0.0000	−3.2357

Table 11
Exact static solutions of the piezoelectric composite laminate (PZT-4/0°/90°/0°/PZT-4) under an applied load (in SI units).

a/h	z/h	$u \cdot 10^{12}$ $(0, \frac{a}{2})$	$v \cdot 10^{12}$ $(\frac{a}{2}, 0)$	$w \cdot 10^{11}$ $(\frac{a}{2}, \frac{a}{2})$	$\phi \cdot 10^{3}$ $(\frac{a}{2}, \frac{a}{2})$	σ_{xz} $(0, \frac{a}{2})$	σ_{yz} $(\frac{a}{2}, 0)$	σ_{zz} $(\frac{a}{2}, \frac{a}{2})$	σ_{xx} $(\frac{a}{2}, \frac{a}{2})$	σ_{yy} $(\frac{a}{2}, \frac{a}{2})$	σ_{xy} $(0, 0)$	$D_x \cdot 10^{12}$ $(0, \frac{a}{2})$	$D_y \cdot 10^{12}$ $(\frac{a}{2}, 0)$	$D_z \cdot 10^{12}$ $(\frac{a}{2}, \frac{a}{2})$
4	1/2	−0.4895	−0.5135	0.3131	0.0000	0.0000	0.0000	1.0000	6.5304	6.6454	−2.4105	0.0000	0.0000	15.650
	2/5	−0.2530	−0.2771	0.3153	0.0576	0.5421	0.5512	0.9529	3.6267	3.7425	−1.2740	181.76	186.26	−0.0327
	2/5	−0.2530	−0.2771	0.3153	0.0576	0.5421	0.5512	0.9529	3.0418	0.7603	−0.2354	−0.1401	−0.1201	−0.0327
	2/15	0.0407	−0.0987	0.3027	0.0570	0.8386	0.6965	0.6633	−0.1667	0.4052	−0.0258	−0.1387	−0.1189	0.0211
	2/15	0.0407	−0.0987	0.3027	0.0570	0.8386	0.6965	0.6633	0.3153	1.2613	−0.0258	−0.1189	−0.1387	0.0211
	0	0.0392	0.0419	0.2972	0.0587	0.8650	0.7463	0.4970	0.2052	−0.2671	0.0360	−0.1225	−0.1429	0.0484
	−2/15	0.0259	0.1848	0.2928	0.0619	0.8745	0.6324	0.3321	0.1054	−1.8168	0.0936	−0.1291	−0.1506	0.0769
	−2/15	0.0259	0.1848	0.2928	0.0619	0.8745	0.6324	0.3321	−0.1890	0.0029	0.0936	−0.1506	−0.1291	0.0769
	−2/5	0.2748	0.3420	0.2856	0.0727	0.5369	0.5621	0.0469	−2.9237	−0.3230	0.2739	−0.1769	−0.1516	0.1401
	−2/5	0.2748	0.3420	0.2856	0.0727	0.5369	0.5621	0.0469	−3.5488	−3.8716	1.4825	156.17	168.70	0.1401
	−1/2	0.4881	0.5548	0.2824	0.0000	0.0000	0.0000	0.0000	−6.1678	−6.4882	2.5065	0.0000	0.0000	−13.728
10	1/2	−6.5396	−6.9134	5.3701	0.0000	0.0000	0.0000	1.0000	32.727	33.445	−12.933	0.0000	0.0000	12.650
	2/5	−4.8721	−5.2463	5.3878	0.4003	1.2562	1.2788	0.9583	24.618	25.337	−9.7270	380.44	391.65	−0.0312
	2/5	−4.8721	−5.2463	5.3878	0.4003	1.2562	1.2788	0.9583	21.129	2.6544	−1.7972	−0.3898	−0.3341	−0.0312
	2/15	−1.2853	−1.7812	5.3962	0.4003	2.4635	1.5306	0.6735	5.7576	1.0442	−0.5447	−0.3897	−0.3340	0.0294
	2/15	−1.2853	−1.7812	5.3962	0.4003	2.4635	1.5306	0.6735	0.9162	7.7892	−0.5447	−0.3340	−0.3897	0.0294
	0	0.0557	0.0907	5.3933	0.4025	2.4981	1.6997	0.5005	0.2224	−0.2039	0.0260	−0.3359	−0.3919	0.0598
	−2/15	1.3915	1.9629	5.3864	0.4063	2.4800	1.5113	0.3275	−0.4696	−8.1974	0.5958	−0.3390	−0.3955	0.0904
	−2/15	1.3915	1.9629	5.3864	0.4063	2.4800	1.5113	0.3275	−5.8566	−0.6170	0.5958	−0.3955	−0.3390	0.0904
	−2/5	4.9565	5.4140	5.3584	0.4185	1.2638	1.2914	0.0420	−21.136	−2.2210	1.8420	−0.4074	−0.3492	0.1528
	−2/5	4.9565	5.4140	5.3584	0.4185	1.2638	1.2914	0.0420	−24.649	−25.528	9.9695	373.18	386.89	0.1528
	−1/2	6.6147	7.0716	5.3396	0.0000	0.0000	0.0000	0.0000	−32.712	−33.590	13.157	0.0000	0.0000	−12.337

Table 12
Exact static solutions of the piezoelectric composite laminate (PZT-4/0°/90°/0°/PZT-4) under an applied potential (in SI units).

a/h	z/h	$u \cdot 10^{12}$ $(0, \frac{a}{2})$	$v \cdot 10^{12}$ $(\frac{a}{2}, 0)$	$w \cdot 10^{11}$ $(\frac{a}{2}, \frac{a}{2})$	ϕ $(\frac{a}{2}, \frac{a}{2})$	σ_{xz} $(0, \frac{a}{2})$	σ_{yz} $(\frac{a}{2}, 0)$	σ_{zz} $(\frac{a}{2}, \frac{a}{2})$	σ_{xx} $(\frac{a}{2}, \frac{a}{2})$	σ_{yy} $(\frac{a}{2}, \frac{a}{2})$	σ_{xy} $(0, 0)$	$D_x \cdot 10^8$ $(0, \frac{a}{2})$	$D_y \cdot 10^8$ $(\frac{a}{2}, 0)$	$D_z \cdot 10^8$ $(\frac{a}{2}, \frac{a}{2})$
4	1/2	−32.461	−28.943	−1.5650	1.0000	0.0000	0.0000	0.0000	112.68	95.779	−147.57	−152.21	−152.21	−24.183
	2/5	5.0703	8.6139	−1.3523	0.9930	5.7957	4.4650	−0.7857	−79.342	−96.367	32.887	−150.85	−150.92	−0.4188
	2/5	5.0703	8.6139	−1.3523	0.9930	5.7957	4.4650	−0.7857	−55.001	−8.7343	6.0763	−0.2417	−0.2072	−0.4188
	2/15	1.6080	3.3055	−1.4096	0.6134	−2.0500	2.3233	−1.7107	−18.085	−3.9834	2.1818	−0.1493	−0.1280	−0.3433
	2/15	1.6080	3.3055	−1.4096	0.6134	−2.0500	2.3233	−1.7107	−2.8884	−35.472	2.1818	−0.1280	−0.1493	−0.3433
	0	0.9736	1.6621	−1.4100	0.4477	−2.4738	−0.5933	−1.5459	−1.9333	−18.116	1.1704	−0.0934	−0.1090	−0.3183
	−2/15	0.4633	0.5086	−1.4052	0.2927	−2.7123	−1.9004	−1.1305	−1.0587	−5.8132	0.4316	−0.0611	−0.0712	−0.3008
	−2/15	0.4633	0.5086	−1.4052	0.2927	−2.7123	−1.9004	−1.1305	−5.3493	−1.0879	0.4316	−0.0712	−0.0611	−0.3008
	−2/5	−1.2088	−0.9850	−1.3883	−0.0001	−1.9391	−1.8550	−0.1673	12.768	0.9991	−0.9741	0.0000	0.0000	−0.2870
	−2/5	−1.2088	−0.9850	−1.3883	−0.0001	−1.9391	−1.8550	−0.1673	10.559	9.4835	−5.2723	−0.0855	−0.0813	−0.2870
	−1/2	−2.2532	−2.0310	−1.3728	0.0000	0.0000	0.0000	0.0000	23.370	22.303	−10.296	0.0000	0.0000	−0.2799
10	1/2	−13.207	−12.615	−1.2650	1.0000	0.0000	0.0000	0.0000	16.993	15.856	−24.823	−60.885	−60.885	−4.1679
	2/5	1.9882	2.5802	−1.2265	0.9987	0.3625	0.3268	−0.0208	−14.335	−15.473	4.3918	−60.787	−60.789	−0.3465
	2/5	1.9882	2.5802	−1.2265	0.9987	0.3625	0.3268	−0.0208	−8.5253	−1.0483	0.8114	−0.0972	−0.0833	−0.3465
	2/15	0.9345	1.3537	−1.2383	0.6575	−0.2067	0.2090	−0.0464	−4.0317	−0.5588	0.4064	−0.0640	−0.0549	−0.3340
	2/15	0.9345	1.3537	−1.2383	0.6575	−0.2067	0.2090	−0.0464	−0.4506	−5.7490	0.4064	−0.0549	−0.0640	−0.3340
	0	0.4973	0.8113	−1.2410	0.4910	−0.2348	0.0038	−0.0412	−0.2554	−3.4453	0.2324	−0.0410	−0.0478	−0.3297
	−2/15	0.0668	0.3046	−1.2421	0.3264	−0.2477	−0.1013	−0.0286	−0.0617	−1.2885	0.0660	−0.0272	−0.0318	−0.3266
	−2/15	0.0668	0.3046	−1.2421	0.3264	−0.2477	−0.1013	−0.0286	−0.3144	−0.1231	0.0660	−0.0318	−0.0272	−0.3266
	−2/5	−0.8773	−0.6625	−1.2399	0.0002	−0.0984	−0.0855	−0.0033	3.7183	0.2947	−0.2735	0.0000	0.0000	−0.3241
	−2/5	−0.8773	−0.6625	−1.2399	0.0002	−0.0984	−0.0855	−0.0033	0.3484	−0.0643	−1.4802	−0.0154	−0.0148	−0.3241
	−1/2	−1.2623	−1.0478	−1.2337	0.0000	0.0000	0.0000	0.0000	2.2205	1.8083	−2.2208	0.0000	0.0000	−0.3236

Table 13
Exact static solutions of the piezoelectric composite laminate (PVDF/90°/0°/90°/PVDF) under an applied load (in SI units); in part, shown by Heyliger et al. [40].

a/h	z/h	$u \cdot 10^{12}$ $(0, \frac{a}{2})$	$v \cdot 10^{12}$ $(\frac{a}{2}, 0)$	$w \cdot 10^{11}$ $(\frac{a}{2}, \frac{a}{2})$	$\phi \cdot 10^{3}$ $(\frac{a}{2}, \frac{a}{2})$	σ_{xz} $(0, \frac{a}{2})$	σ_{yz} $(\frac{a}{2}, 0)$	σ_{zz} $(\frac{a}{2}, \frac{a}{2})$	σ_{xx} $(\frac{a}{2}, \frac{a}{2})$	σ_{yy} $(\frac{a}{2}, \frac{a}{2})$	σ_{xy} $(0, 0)$	$D_x \cdot 10^{12}$ $(0, \frac{a}{2})$	$D_y \cdot 10^{12}$ $(\frac{a}{2}, 0)$	$D_z \cdot 10^{12}$ $(\frac{a}{2}, \frac{a}{2})$
4	1/2	−0.5301	−0.7759	0.3791	0.0000	0.0000	0.0000	1.0000	10.335	1.7726	−0.6595	0.0000	0.0000	−1.2758
	2/5	−0.3181	−0.5201	0.3722	0.2785	0.6756	0.1587	0.9647	6.2992	1.2367	−0.4233	−3.9568	−3.0595	−0.9899
	2/5	−0.3181	−0.5201	0.3722	0.2785	0.6756	0.1587	0.9647	0.8554	5.8445	−0.3722	−0.5810	−0.6778	−0.9899
	2/15	−0.1248	−0.0268	0.3606	0.1909	0.8526	0.8117	0.6803	0.4495	0.5500	−0.0673	−0.3982	−0.4646	−0.7695
	2/15	−0.1248	−0.0268	0.3606	0.1909	0.8526	0.8117	0.6803	1.5539	0.3863	−0.0673	−0.4646	−0.3982	−0.7695
	0	0.0368	0.0409	0.3553	0.1544	0.9223	0.8441	0.4987	−0.2140	0.2056	0.0345	−0.3757	−0.3221	−0.6879
	−2/15	0.1994	0.0968	0.3507	0.1215	0.8005	0.8480	0.3180	−1.9888	0.0352	0.1315	−0.2958	−0.2536	−0.6227
	−2/15	0.1994	0.0968	0.3507	0.1215	0.8005	0.8480	0.3180	−0.0310	−0.9376	0.1315	−0.2536	−0.2958	−0.6227
	−2/5	0.3614	0.5466	0.3426	0.0639	0.7026	0.1477	0.0356	−0.4004	−5.7705	0.4032	−0.1332	−0.1554	−0.5357
	−2/5	0.3614	0.5466	0.3426	0.0639	0.7026	0.1477	0.0356	−6.8924	−1.0979	0.4585	−2.1520	−1.2193	−0.5357
	−1/2	0.5444	0.7784	0.3406	0.0000	0.0000	0.0000	0.0000	−10.381	−1.5819	0.6680	0.0000	0.0000	−0.3939
10	1/2	−8.2443	−9.0228	6.7157	0.0000	0.0000	0.0000	1.0000	62.792	7.7540	−3.4880	0.0000	0.0000	−0.9744
	2/5	−6.3519	−6.9887	6.7171	0.5644	1.8357	0.3131	0.9648	48.426	6.0402	−2.6948	−6.1349	−3.3381	−0.8201
	2/5	−6.3519	−6.9887	6.7171	0.5644	1.8357	0.3131	0.9648	3.2054	30.066	−2.3695	−0.4710	−0.5495	−0.8201
	2/15	−2.2088	−1.9843	6.7326	0.4862	2.1512	2.0438	0.6836	1.2513	8.7167	−0.7448	−0.4057	−0.4733	−0.7406
	2/15	−2.2088	−1.9843	6.7326	0.4862	2.1512	2.0438	0.6836	9.6366	1.1934	−0.7448	−0.4733	−0.4057	−0.7406
	0	0.0700	0.0695	6.7306	0.4499	2.3648	2.0884	0.5007	−0.1181	0.2195	0.0248	−0.4380	−0.3754	−0.7052
	−2/15	2.3481	2.1182	6.7228	0.4153	2.1392	2.0601	0.3177	−9.8697	−0.7526	0.7933	−0.4043	−0.3466	−0.6724
	−2/15	2.3481	2.1182	6.7228	0.4153	2.1392	2.0601	0.3177	−0.8119	−8.9277	0.7933	−0.3466	−0.4043	−0.6724
	−2/5	6.4713	7.1030	6.6878	0.3508	1.8570	0.3112	0.0355	−2.7581	−30.194	2.4110	−0.2927	−0.3415	−0.6145
	−2/5	6.4713	7.1030	6.6878	0.3508	1.8570	0.3112	0.0355	−49.109	−5.9379	2.7421	−5.4404	−2.6170	−0.6145
	−1/2	8.3508	9.1271	6.6774	0.0000	0.0000	0.0000	0.0000	−63.377	−7.6429	3.5306	0.0000	0.0000	−0.4825

Table 14
Exact static solutions of the piezoelectric composite laminate (PVDF/90°/0°/90°/PVDF) under an applied potential (in SI units); in part, shown by Heyliger et al. [40].

a/h	z/h	$u \cdot 10^{13}$ $(0, \frac{a}{2})$	$v \cdot 10^{13}$ $(\frac{a}{2}, 0)$	$w \cdot 10^{12}$ $(\frac{a}{2}, \frac{a}{2})$	ϕ $(\frac{a}{2}, \frac{a}{2})$	$\sigma_{xz} \cdot 10^{2}$ $(0, \frac{a}{2})$	$\sigma_{yz} \cdot 10^{2}$ $(\frac{a}{2}, 0)$	$\sigma_{zz} \cdot 10^{2}$ $(\frac{a}{2}, \frac{a}{2})$	$\sigma_{xx} \cdot 10$ $(\frac{a}{2}, \frac{a}{2})$	$\sigma_{yy} \cdot 10$ $(\frac{a}{2}, \frac{a}{2})$	$\sigma_{xy} \cdot 10$ $(0, 0)$	$D_x \cdot 10^{9}$ $(0, \frac{a}{2})$	$D_y \cdot 10^{9}$ $(\frac{a}{2}, 0)$	$D_z \cdot 10^{9}$ $(\frac{a}{2}, \frac{a}{2})$
4	1/2	−0.4643	0.5861	1.2758	1.0000	0.0000	0.0000	0.0000	−25.243	−42.687	0.0615	−8.6944	−8.3346	−5.2861
	2/5	−1.5054	−1.7490	0.2075	0.9592	−8.6801	−26.955	1.6395	3.2423	−27.743	−1.6435	−8.3396	−7.9934	−3.9772
	2/5	−1.5054	−1.7490	0.2075	0.9592	−8.6801	−26.955	1.6395	1.7155	18.635	−1.4451	−2.0011	−2.3347	−3.9772
	2/15	−0.6095	−0.7781	0.2195	0.5995	−3.9058	1.1331	5.2068	0.9346	8.4394	−0.6162	−1.2507	−1.4592	−3.2452
	2/15	−0.6095	−0.7781	0.2195	0.5995	−3.9058	1.1331	5.2068	6.7126	1.0434	−0.6162	−1.4592	−1.2507	−3.2452
	0	−0.3645	−0.6192	0.2201	0.4431	2.1796	2.6658	5.0696	4.1162	0.8518	−0.4368	−1.0785	−0.9244	−2.9989
	−2/15	−0.2346	−0.5106	0.2197	0.2973	6.0668	3.8691	4.2795	2.7082	0.6938	−0.3309	−0.7235	−0.6201	−2.8241
	−2/15	−0.2346	−0.5106	0.2197	0.2973	6.0668	3.8691	4.2795	0.5158	5.5352	−0.3309	−0.6201	−0.7235	−2.8241
	−2/5	−0.2836	−0.4959	0.2206	0.0235	7.6575	14.925	0.8611	0.3845	5.2690	−0.3461	−0.0490	−0.0571	−2.6734
	−2/5	−0.2836	−0.4959	0.2206	0.0235	7.6575	14.925	0.8611	−11.611	−20.106	−0.3937	−0.2042	−0.1963	−2.6734
	−1/2	−0.4545	−0.9503	−0.3939	0.0000	0.0000	0.0000	0.0000	−8.2111	−19.118	−0.7094	0.0000	0.0000	−2.6577
10	1/2	−1.1452	−1.0928	0.9744	1.0000	0.0000	0.0000	0.0000	−13.605	−26.632	−0.4521	−3.4777	−3.3338	−3.4903
	2/5	−1.6255	−2.1655	0.1934	0.9702	−3.3161	−7.7775	0.1810	−8.5482	−24.123	−0.7658	−3.3739	−3.2340	−3.2795
	2/5	−1.6255	−2.1655	0.1934	0.9702	−3.3161	−7.7775	0.1810	0.7373	9.1874	−0.6733	−0.8096	−0.9445	−3.2795
	2/15	−1.2542	−1.8136	0.2043	0.6475	−2.2475	−0.2943	0.7413	0.6104	7.7069	−0.5449	−0.5403	−0.6304	−3.1572
	2/15	−1.2542	−1.8136	0.2043	0.6475	−2.2475	−0.2943	0.7413	5.4151	0.7548	−0.5449	−0.6304	−0.5403	−3.1572
	0	−1.1431	−1.7260	0.2091	0.4901	0.1350	0.2344	0.7859	4.9454	0.7182	−0.5096	−0.4772	−0.4090	−3.1141
	−2/15	−1.0842	−1.6555	0.2135	0.3347	2.3542	0.7366	0.7130	4.6908	0.6858	−0.4866	−0.3258	−0.2793	−3.0829
	−2/15	−1.0842	−1.6555	0.2135	0.3347	2.3542	0.7366	0.7130	0.5384	7.0315	−0.4866	−0.2793	−0.3258	−3.0829
	−2/5	−1.1073	−1.6543	0.2221	0.0269	3.2011	6.9407	0.1585	0.5186	7.0081	−0.4905	−0.0225	−0.0262	−3.0555
	−2/5	−1.1073	−1.6543	0.2221	0.0269	3.2011	6.9407	0.1585	−11.045	−22.789	−0.5579	−0.0937	−0.0901	−3.0555
	−1/2	−1.1938	−1.8760	−0.4825	0.0000	0.0000	0.0000	0.0000	−10.359	−22.597	−0.6201	0.0000	0.0000	−3.0527

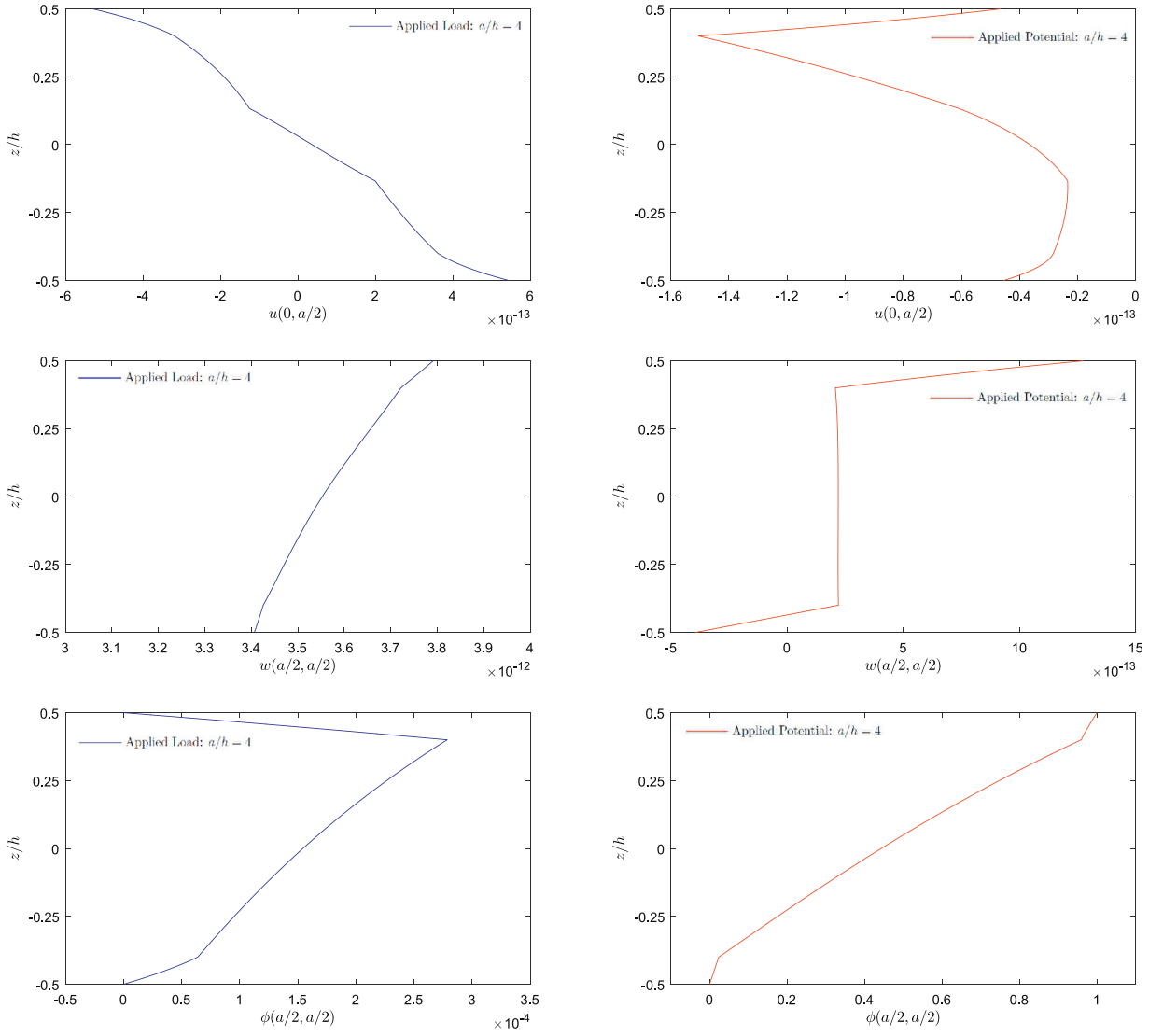

Fig. 4. Exact static solutions of the piezoelectric composite laminate (PVDF/90°/0°/90°/PVDF) under an applied load or electric potential, using $a/h = 4$: through-thickness distributions of displacements and electric potential (in SI units).

In all Tables 9,10,11,12,13,14 alike, the exact static solutions provide a detailed through-thickness evaluation of all displacements and stresses, together with the electric potential and all electric displacements, considering two distinct side-to-thickness ratios $a/h = 4, 10$, thus including both thick and moderately thick plates. This comprehensive evaluation for each of the three piezoelectric composite laminates, in both sensor and actuator configurations, ends up adding much to the original benchmarks by Heyliger [5] as well as Heyliger et al. [40] concerning two of these piezoelectric composite laminates. In fact, in these original works, no graphical description is presented for any of the two piezoelectric composite laminates. Hence, in the interest of a more clear understanding of the static behaviour of piezoelectric composite laminates, Figs. 4 and 5 demonstrate, for the laminate (PVDF/90°/0°/90°/PVDF) as an example, the exact through-thickness distributions of main electric and elastic field variables, considering an applied load or electric potential, side-by-side. Actually, Figs. 4 and 5 include only one side-to-thickness ratio $a/h = 4$, as characteristic of thick plates, which typically exhibit more intricate through-thickness distributions.

All together, Figs. 4 and 5 provide a broad perception of the static behaviour of a piezoelectric composite laminate, namely (PVDF/90°/0°/90°/PVDF), enlightening the distinction between sensor and actuator configurations, as it affects the corresponding through-thickness distributions of main electric and elastic field variables. From a modelling viewpoint, all through-thickness effects exhibited in both configurations must be captured accurately, thus the aforementioned C_z^0 interlaminar continuity requirements of displacements and transverse stresses must be extended to the electric potential and transverse electric displacement. Besides, within each layer, a high-order variable description, in general, seems most suitable, especially when thick plates are considered.

Furthermore, 3D exact free vibration solutions of each of the three piezoelectric composite laminates are shown in Tables 15,16,17. In essence, the free vibration solutions reveal the first twenty natural frequencies, along with the associated modes of natural vibration, considering two distinct side-to-thickness ratios $a/h = 4, 10$, thus including again thick and moderately thick plates. More precisely, for each natural frequency, the corresponding in-plane mode (n_x, n_y) is reported, including *special modes* for either $n_x = 0$ or $n_y = 0$, together with the *thickness mode* number of each pair (n_x, n_y).

An additional remark is appropriate at this point, since in agreement with the leading work by Heyliger and Saravanos [7] on exact free vibration solutions of piezoelectric composite laminates, an equal density of a unit value is assumed for every layer, as in $\rho = 1$ kg/m^3, as stated

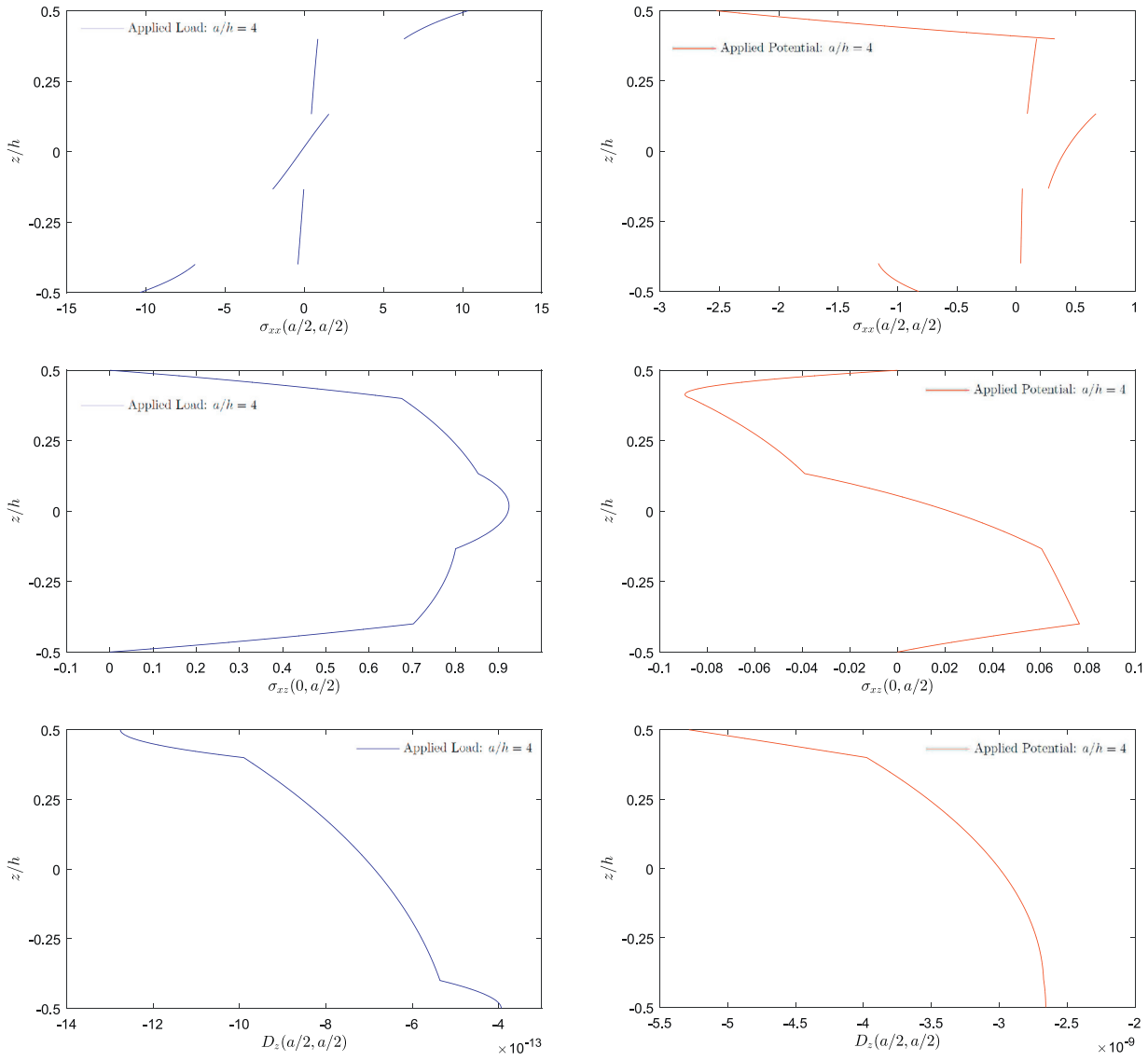

Fig. 5. Exact static solutions of the piezoelectric composite laminate (PVDF/90°/0°/90°/PVDF) under an applied load or electric potential, using $a/h = 4$: through-thickness distributions of stresses and electric displacements (in SI units).

Table 15
Exact free vibration solutions of the piezoelectric composite laminate (PZT-4/0°/90°/PZT-4): first twenty natural frequencies (in units of 10^3 rad/s) and associated modes (n_x, n_y)–N_z (in-plane mode and thickness mode number).

a/h	ω_1	ω_2	ω_3	ω_4	ω_5	ω_6	ω_7	ω_8	ω_9	ω_{10}
	ω_{11}	ω_{12}	ω_{13}	ω_{14}	ω_{15}	ω_{16}	ω_{17}	ω_{18}	ω_{19}	ω_{20}
4	56.685	80.444	80.444	103.670	103.670	137.144	156.511	156.511	157.620	157.620
	(1,1)–1	**(0,1)**–1	**(1,0)**–1	(1,2)–1	(2,1)–1	(2,2)–1	(1,3)–1	(3,1)–1	**(0,2)**–1	**(2,0)**–1
	181.552	181.552	184.178	211.307	211.307	218.196	229.268	229.268	229.328	229.328
	(2,3)–1	(3,2)–1	(1,1)–**2**	(1,4)–1	(4,1)–1	(3,3)–1	**(0,1)**–**2**	**(1,0)**–**2**	**(0,3)**–1	**(3,0)**–1
10	13.000	28.754	28.754	32.372	32.372	40.988	48.998	48.998	58.407	58.407
	(1,1)–1	(1,2)–1	(2,1)–1	**(0,1)**–1	**(1,0)**–1	(2,2)–1	(1,3)–1	(3,1)–1	(2,3)–1	(3,2)–1
	64.521	64.521	70.732	70.732	72.691	78.237	78.237	79.883	90.004	90.004
	(0,2)–1	**(2,0)**–1	(1,4)–1	(4,1)–1	(3,3)–1	(2,4)–1	(4,2)–1	(1,1)–**2**	(3,4)–1	(4,3)–1

in Table 2. This is done similarly for all three piezoelectric composite laminates, including one original benchmark shown by Heyliger and Saravanos [7]. Even so, as most useful for future assessments, the scope of the exact free vibration solutions provided here is not actually limited to this density value alone, so long as an equal density is kept for every layer of the laminate. To be precise, if another density value is of interest, as in ρ', the corresponding natural frequencies ω' can be readily determined by a multiplying factor i.e. $\omega' = \omega\sqrt{\rho/\rho'}$, for each same case of square plate geometry (a and h), rather in line with Eq. (62).

Examining closely Tables 15,16,17, it is evident that *special modes* are, once again, a significant part of the first twenty natural modes of vibration of each (simply supported) piezoelectric composite laminate, particularly when thick plates are considered. In such case, among the first twenty modes of vibration of each piezoelectric composite lami-

Table 16
Exact free vibration solutions of the piezoelectric composite laminate (PZT-4/0°/90°/0°/PZT-4): first twenty natural frequencies (in units of 10^5 rad/s) and associated modes (n_x, n_y)–N_z (in-plane mode and thickness mode number); in part, shown by Heyliger and Saravanos [7].

	ω_1	ω_2	ω_3	ω_4	ω_5	ω_6	ω_7	ω_8	ω_9	ω_{10}
a/h	ω_{11}	ω_{12}	ω_{13}	ω_{14}	ω_{15}	ω_{16}	ω_{17}	ω_{18}	ω_{19}	ω_{20}
4	57.074	80.330	80.555	101.421	105.244	136.604	152.192	156.766	158.412	159.576
	(1,1)–1	**(1,0)**–1	**(0,1)**–1	(1,2)–1	(2,1)–1	(2,2)–1	(1,3)–1	**(2,0)**–1	**(0,2)**–1	(3,1)–1
	178.693	183.055	191.301	204.883	217.262	217.402	226.148	226.874	228.490	231.486
	(2,3)–1	(3,2)–1	(1,1)–**2**	(1,4)–1	(4,1)–1	(3,3)–1	(2,4)–1	**(3,0)**–1	**(0,1)**–**2**	**(1,0)**–**2**
10	13.526	27.822	30.949	32.365	32.380	41.578	47.104	51.608	57.615	59.845
	(1,1)–1	(1,2)–1	(2,1)–1	**(1,0)**–1	**(0,1)**–1	(2,2)–1	(1,3)–1	(3,1)–1	(2,3)–1	(3,2)–1
	64.462	64.579	68.181	72.843	73.217	76.453	78.109	79.959	89.049	89.801
	(2,0)–1	**(0,2)**–1	(1,4)–1	(3,3)–1	(4,1)–1	(2,4)–1	(1,1)–**2**	(4,2)–1	(3,4)–1	(1,5)–1

Table 17
Exact free vibration solutions of the piezoelectric composite laminate (PVDF/90°/0°/90°/PVDF): first twenty natural frequencies (in units of 10^5 rad/s) and associated modes (n_x, n_y)–N_z (in-plane mode and thickness mode number).

	ω_1	ω_2	ω_3	ω_4	ω_5	ω_6	ω_7	ω_8	ω_9	ω_{10}
a/h	ω_{11}	ω_{12}	ω_{13}	ω_{14}	ω_{15}	ω_{16}	ω_{17}	ω_{18}	ω_{19}	ω_{20}
4	52.241	59.859	59.859	93.081	98.627	119.712	119.713	125.243	141.135	148.353
	(1,1)–1	**(0,1)**–1	**(1,0)**–1	(1,2)–1	(2,1)–1	**(0,2)**–1	**(2,0)**–1	(2,2)–1	(1,3)–1	(3,1)–1
	164.142	167.209	179.552	179.555	191.439	197.933	198.717	208.960	213.130	215.013
	(2,3)–1	(3,2)–1	**(0,3)**–1	**(3,0)**–1	(1,4)–1	(3,3)–1	(4,1)–1	(2,4)–1	(4,2)–1	**(1,0)**–**2**
10	12.113	23.944	23.944	26.010	29.515	37.899	44.470	47.888	47.888	50.294
	(1,1)–1	**(0,1)**–1	**(1,0)**–1	(1,2)–1	(2,1)–1	(2,2)–1	(1,3)–1	**(0,2)**–1	**(2,0)**–1	(3,1)–1
	52.604	55.832	64.093	66.815	70.165	71.397	71.831	71.831	75.507	81.438
	(2,3)–1	(3,2)–1	(1,4)–1	(3,3)–1	(2,4)–1	(4,1)–1	**(0,3)**–1	**(3,0)**–1	(4,2)–1	(3,4)–1

nate, about seven or eight modes correspond to *special modes*. In detail, for thick plates most notably, the second and third lowest natural frequencies typically correspond to *special modes*, namely either the pair (0,1) or (1,0), as demonstrated in all Tables 15–17. Thus, *special modes* of (simply supported) piezoelectric composite laminates clearly cannot be overlooked, though naturally, the relevance of *special modes* tends to subside somewhat as the plate becomes less thick. Along with this, Tables 15–17 also indicate that for thick plates, in particular, at least up to the second *thickness mode* can appear among the first twenty modes of vibration of each piezoelectric composite laminate. Specifically, for each thick laminate considered, about one up to three modes of vibration among the first twenty modes correspond to a second *thickness mode*. Actually, comparing the free vibration behaviour of two analogous piezoelectric composite laminates as shown in Tables 16 and 17, suggests that laminates involving PZT-4 (as opposed to PVDF) are apparently more susceptible to the occurrence of a second (or higher) *thickness mode* among the lower natural frequencies. This laminate free vibration behaviour is therefore further characterized in Fig. 6, in line with the aforementioned Table 16.

As intended, Fig. 6 provides some more insight into a few modes of natural vibration, namely, the first few through-thickness mode shapes of each in-plane mode (n_x, n_y). More precisely, it displays for the in-plane mode (1,1), the first four *thickness modes* of the transverse displacement w, and similarly for the in-plane mode (2,1), the first two *thickness modes*. As already seen before, Fig. 6 also reveals that, for each in-plane mode as (1,1) or (2,1), the natural modes of vibration from the second *thickness mode* onwards, rather expose the transverse normal compressibility of the laminate. Further to this, the *thickness modes* of the transverse displacement w, apparently can be divided into either symmetric or antisymmetric modes with respect to the plate mid-surface, while exhibiting such transverse normal compressibility, as clearly manifested by the first four *thickness modes* of the in-plane mode (1,1). Other than that, Fig. 6 also displays for the *special mode* (0,1), the first two *thickness modes* of the in-plane displacement u. Thus, it demonstrates that, for each *special mode* as (0,1) or (1,0), the natural modes of vibration from the second *thickness mode* onwards, expose also the effect of transverse shear of the laminate. Ultimately, the importance of *thickness modes*, from the second onwards, among the first twenty, or more, modes of vibration of any piezoelectric composite laminate seems to be most influenced by the degree of sensitivity to the effects of transverse shear and normal compressibility of the plate, which are naturally much more pronounced when thick plates are considered.

5. Conclusions

As cutting-edge structural design technology unfolds, pushing forward the capabilities of multilayered piezoelectric and/or composite plates, 3D exact solutions continue to be a cornerstone in the accuracy assessment of the most advanced theories and finite element models, relying much on benchmarking. This work on 3D exact electroelastic static and free vibration solutions of multilayered plates provides a comprehensive evaluation of well-known benchmarks for piezoelectric and/or composite laminates as well as soft core sandwich plates, adding much to thus far available in the literature. The exact solution method for simply supported multilayered plates is fully described in line with earlier leading works, compiled in a single study in a consistent form throughout. It considers *extension mode* piezoelectric layers and/or purely elastic layers, such as composite layers, including all particularities arising from an orthotropic, transversely isotropic or simply isotropic layer. Furthermore, within the free vibration solution, not only *thickness modes* are addressed for each in-plane mode (n_x, n_y), but also the so-called *special modes* for either $n_x = 0$ or $n_y = 0$ are here purposely highlighted, though often overlooked.

The benchmarks for each multilayered plate cover both static and free vibration solutions, divided into purely elastic solutions, as in composite laminates and soft core sandwich plates, or else, electro-elastic solutions, namely piezoelectric composite laminates, considering not only but especially thick plates. For each multilayered plate, the static solution considers either a bi-sinusoidal applied load or a bi-sinusoidal applied electric potential, providing a detailed through-thickness evaluation of displacements and stresses, and when present, the electric potential and electric displacements. In fact, through-thickness distributions are also demonstrated to further characterize the static behaviour of a soft core sandwich plate as well as a piezoelectric composite lam-

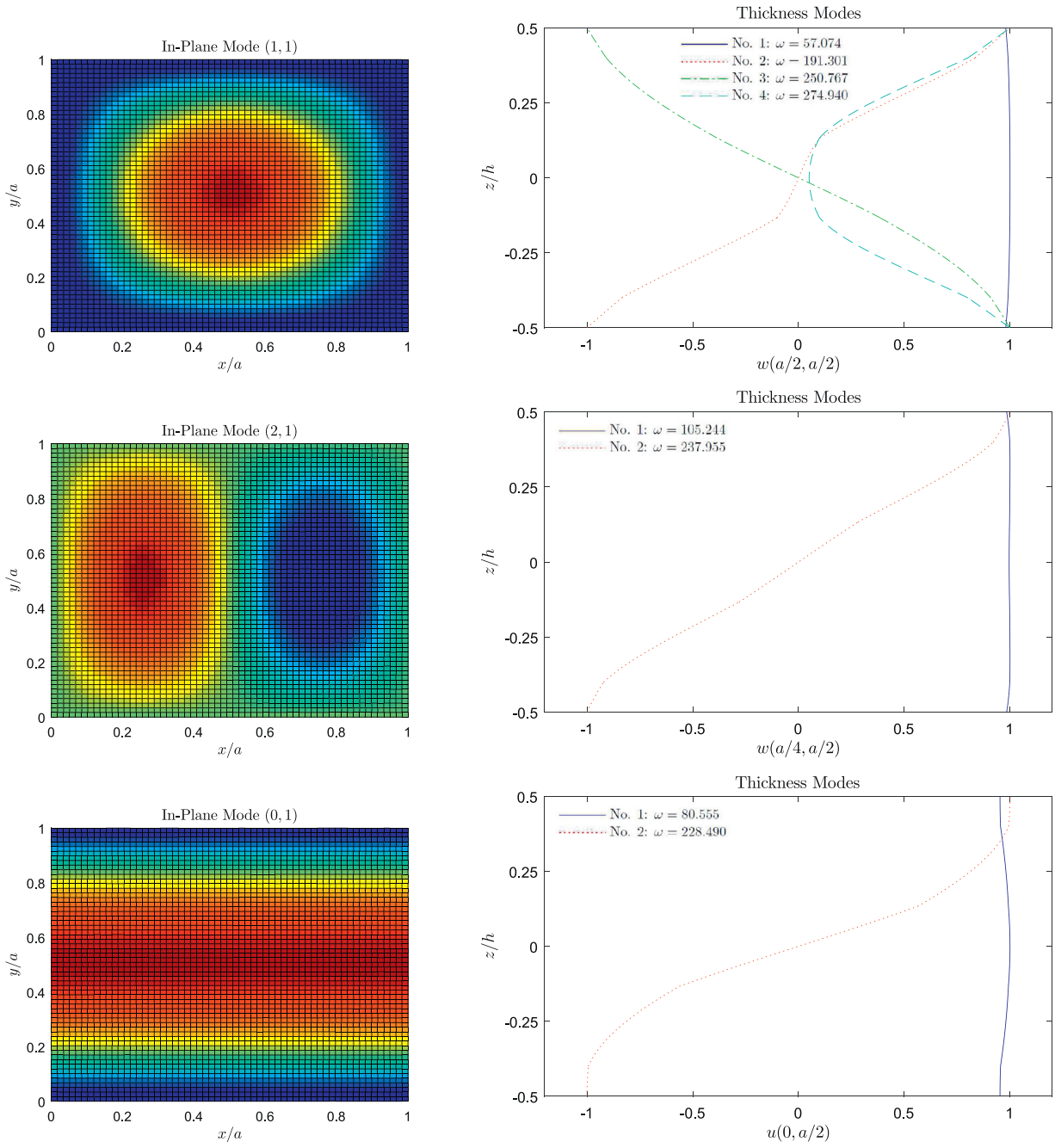

Fig. 6. Exact free vibration solutions of the piezoelectric composite laminate (PZT-4/0°/90°/0°/PZT-4), using $a/h = 4$: a few natural frequencies (in units of 10^5 rad/s) and associated modes, characterizing the first few through-thickness modes of each in-plane mode.

inate, enlightening the distinction between sensor and actuator configurations. The respective free vibration solution reveals the first twenty natural frequencies and associated modes, including all together *special modes* and *thickness modes*. Most especially, for (simply supported) thick plates, among the first twenty modes of vibration, typically around 35% is associated with *special modes* and around 15% corresponds to a second *thickness mode*. Actually, the second and third lowest natural frequencies are often associated with *special modes*, namely (0,1) and (1,0), thus clearly cannot be disregarded. In addition, a few through-thickness modes are also displayed to further characterize the free vibration behaviour of a soft core sandwich plate as well as a piezoelectric composite laminate. In the end, the significance of *thickness modes*, from the second onwards, seems to be most influenced by the degree of sensitivity to the effects of transverse shear and normal compressibility of the plate. This gives reason to the relevance of *thickness modes* when thick plates are considered, and most especially sandwich plates exhibiting high core compressibility.

Data availability

The raw/processed data required to reproduce these findings cannot be shared at this time as the data also forms part of an ongoing study.

Declaration of Competing Interest

The authors declare that they have no known competing financial interests or personal relationships that could have appeared to influence the work reported in this paper.

Acknowledgements

The authors acknowledge the financial support received through National Funds from "Fundação para a Ciência e a Tecnologia" (FCT) via IDMEC, under the Associated Laboratory of Energy, Transports and Aeronautics (LAETA), Project UIDB/50022/2020.

References

[1] N.J. Pagano, Exact solutions for rectangular bidirectional composites and sandwich plates, J. Compos. Mater. 4 (1970) 20–34, doi:10.1177/002199837000400102.
[2] N.J. Pagano, S.J. Hatfield, Elastic behavior of multilayered bidirectional composites, AIAA J. 10 (1972) 931–933, doi:10.2514/3.50249.
[3] A.T. Jones, Exact natural frequencies for cross-ply laminates, J. Compos. Mater. 4 (1970) 476–491, doi:10.1177/002199837000400404.
[4] S. Srinivas, A.K. Rao, Bending, vibration and buckling of simply supported thick orthotropic rectangular plates and laminates, Int. J. Solids Struct. 6 (1970) 1463–1481, doi:10.1016/0020-7683(70)90076-4.
[5] P. Heyliger, Static behavior of laminated elastic/piezoelectric plates, AIAA J. 32 (1994) 2481–2484, doi:10.2514/3.12321.
[6] P. Heyliger, Exact solutions for simply supported laminated piezoelectric plates, J. Appl. Mech. 64 (1997) 299–306, doi:10.1115/1.2787307.
[7] P. Heyliger, D.A. Saravanos, Exact free-vibration analysis of laminated plates with embedded piezoelectric layers, J. Acoust. Soc. Am. 98 (1995) 1547–1557, doi:10.1121/1.413420.
[8] S.S. Vel, R.C. Batra, Exact solution for rectangular sandwich plates with embedded piezoelectric shear actuators, AIAA J. 39 (2001) 1363–1373, doi:10.2514/2.1455.
[9] B.P. Baillargeon, S.S. Vel, Exact solution for the vibration and active damping of composite plates with piezoelectric shear actuators, J. Sound Vib. 282 (2005) 781–804, doi:10.1016/j.jsv.2004.03.042.
[10] R.C. Batra, S. Aimmanee, Missing frequencies in previous exact solutions of free vibrations of simply supported rectangular plates, J. Sound Vib. 265 (2003) 887–896, doi:10.1016/S0022-460X(02)01568-7.
[11] J.F. Deü, A. Benjeddou, Free-vibration analysis of laminated plates with embedded shear-mode piezoceramic layers, Int. J. Solids Struct. 42 (2005) 2059–2088, doi:10.1016/j.ijsolstr.2004.09.003.
[12] V.B. Tungikar, K.M. Rao, Three dimensional exact solution of thermal stresses in rectangular composite laminate, Compos. Struct. 27 (1994) 419–430, doi:10.1016/0263-8223(94)90268-2.
[13] K. Xu, A.K. Noor, Y.Y. Tang, Three-dimensional solutions for coupled thermoelectroelastic response of multilayered plates, Comput. Meth. Appl. Mech. Eng. 126 (1995) 355–371, doi:10.1016/0045-7825(95)00825-L.
[14] K. Xu, A.K. Noor, Y.Y. Tang, Three-dimensional solutions for free vibrations of initially-stressed thermoelectroelastic multilayered plates, Comput. Meth. Appl. Mech. Eng. 141 (1997) 125–139, doi:10.1016/S0045-7825(96)01065-1.
[15] F. Moleiro, C.M.M. Soares, C.A.M. Soares, J.N. Reddy, Benchmark exact solutions for the static analysis of multilayered piezoelectric composite plates using PVDF, Compos. Struct. 107 (2014) 389–395, doi:10.1016/j.compstruct.2013.08.019.
[16] F. Moleiro, A.L. Araújo, J.N. Reddy, Benchmark exact free vibration solutions for multilayered piezoelectric composite plates, Compos. Struct. 182 (2017) 598–605, doi:10.1016/j.compstruct.2017.09.035.
[17] F. Moleiro, C.M.M. Soares, E. Carrera, Three-dimensional hygro-thermo-elastic solutions for multilayered plates: composite laminates, fibre metal laminates and sandwich plates, Compos. Struct. 216 (2019) 260–278, doi:10.1016/j.compstruct.2019.02.071.
[18] A.K. Noor, W.S. Burton, Assessment of shear deformation theories for multilayered composite plates, Appl. Mech. Rev. 42 (1989) 1–13, doi:10.1115/1.3152418.
[19] A.K. Noor, W.S. Burton, Computational models for high-temperature multilayered composite plates and shells, Appl. Mech. Rev. 45 (1992) 419–446, doi:10.1115/1.3119742.
[20] T.K. Mallikarjuna, A critical review and some results of recently developed refined theories of fibre-reinforced laminated composites and sandwiches, Compos. Struct. 23 (1993) 293–312, doi:10.1016/0263-8223(93)90230-N.
[21] J.N. Reddy, D.H. Robbins Jr, Theories and computational models for composite laminates, Appl. Mech. Rev. 47 (1994) 147–169, doi:10.1115/1.3111076.
[22] A.K. Noor, W.S. Burton, C.W. Bert, Computational models for sandwich panels and shells, Appl. Mech. Rev. 49 (1996) 155–199, doi:10.1115/1.3101923.
[23] E. Carrera, Theories and finite elements for multilayered anisotropic, composite plates and shells, Arch. Comput. Method Eng. 9 (2002) 87–140, doi:10.1007/BF02736649.
[24] E. Carrera, Theories and finite elements for multilayered anisotropic, composite plates and shells: a unified compact formulation with numerical assessment and benchmarking, Arch. Comput. Method Eng. 10 (2003) 215–296, doi:10.1007/BF02736224.
[25] E. Carrera, Historical review of zig-zag theories for multilayered plates and shells, Appl. Mech. Rev. 56 (2003) 287–308, doi:10.1115/1.1557614.
[26] J.N. Reddy, Mechanics of laminated composite plates and shells: Theory and analysis, second ed., CRC Press, Boca Raton, Florida, 2004.
[27] Y.Y. Tang, A.K. Noor, K. Xu, Assessment of computational models for thermoelectroelastic multilayered plates, Comput. Struct. 61 (1996) 915–933, doi:10.1016/0045-7949(96)00037-5.
[28] D.A. Saravanos, P.R. Heyliger, Mechanics and computational models for laminated piezoelectric beams, plates and shells, Appl. Mech. Rev. 52 (1999) 305–320, doi:10.1115/1.3098918.
[29] S.V. Gopinathan, V.V. Varadan, V.K. Varadan, A review and critique of theories for piezoelectric laminates, Smart Mater. Struct. 9 (2000) 24–48, doi:10.1088/0964-1726/9/1/304.
[30] A. Benjeddou, Advances in piezoelectric finite element modeling of adaptive structural elements: a survey, Comput. Struct. 76 (2000) 347–363, doi:10.1016/S0045-7949(99)00151-0.
[31] M.A. Trindade, A. Benjeddou, Hybrid active-passive damping treatments using viscoelastic and piezoelectric materials: review and assessment, J. Vib. Control 8 (2002) 699–745, doi:10.1177/1077546029186.
[32] I. Chopra, Review of state of art of smart structures and integrated systems, AIAA J. 40 (2002) 2145–2187, doi:10.2514/2.1561.
[33] E. Carrera, S. Brischetto, P. Nali, Plates and shells for smart structures: Classical and advanced theories for modeling and analysis, John Wiley & Sons, Chichester, West Sussex, 2011.
[34] K.M. Liew, Z.Z. Pan, L.W. Zhang, An overview of layerwise theories for composite laminates and structures: development, numerical implementation and application, Compos. Struct. 216 (2019) 240–259, doi:10.1016/j.compstruct.2019.02.074.
[35] S.Q. Zhang, G.Z. Zao, M.N. Rao, R. Schmidt, Y.J. Yu, A review on modeling techniques of piezoelectric integrated plates and shells, J. Intell. Mater. Syst. Struct. 30 (2019) 1133–1147, doi:10.1177/1045389X19836169.
[36] D. Li, Layerwise theories of laminated composite structures and their applications: a review, Arch. Comput. Method Eng. (2020), doi:10.1007/s11831-019-09392-2.
[37] E. Carrera, L. Demasi, Classical and advanced multilayered plate elements based upon PVD and RMVT. part 2: numerical implementations, Int. J. Numer. Methods Eng. 55 (2002) 253–291, doi:10.1002/nme.493.
[38] F. Moleiro, C.M.M. Soares, C.A.M. Soares, J.N. Reddy, A layerwise mixed least-squares finite element model for static analysis of multilayered composite plates, Comput. Struct. 89 (2011) 1730–1742, doi:10.1016/j.compstruc.2010.10.008.
[39] F. Moleiro, C.M.M. Soares, C.A.M. Soares, J.N. Reddy, Layerwise mixed least-squares finite element models for static and free vibration analysis of multilayered composite plates, Compos. Struct. 92 (2010) 2328–2338, doi:10.1016/j.compstruct.2009.07.005.
[40] P. Heyliger, G. Ramirez, D. Saravanos, Coupled discrete-layer finite elements for laminated piezoelectric plates, Commun. Numer. Methods Eng. 10 (1994) 971–981, doi:10.1002/cnm.1640101203.
[41] E. Carrera, A. Büttner, P. Nali, Mixed elements for the analysis of anisotropic multilayered piezoelectric plates, J. Intell. Mater. Syst. Struct. 21 (2010) 701–717, doi:10.1177/1045389X10364864.
[42] F. Moleiro, C.M.M. Soares, C.A.M. Soares, J.N. Reddy, Assessment of a layerwise mixed least-squares model for analysis of multilayered piezoelectric composite plates, Comput. Struct. 108–109 (2012) 14–30, doi:10.1016/j.compstruc.2012.04.002.
[43] F. Moleiro, C.M.M. Soares, C.A.M. Soares, J.N. Reddy, Layerwise mixed models for analysis of multilayered piezoelectric composite plates using least-squares formulation, Compos. Struct. 119 (2015) 134–149, doi:10.1016/j.compstruct.2014.08.031.
[44] F. Moleiro, E. Carrera, G. Li, M. Cinefra, J.N. Reddy, Hygro-thermo-mechanical modelling of multilayered plates: hybrid composite laminates, fibre metal laminates and sandwich plates, Compos. Pt. B-Eng. 177 (2019) 107388, doi:10.1016/j.compositesb.2019.107388.